NASA Contractor Report 172228

Measurement and Analysis of Critical Crack Tip Processes Associated with Variable Amplitude Fatigue Crack Growth

S. J. Hudak, D. L. Davidson, and K. S. Chan
Southwest Research Institute
San Antonio, Texas

Contract NAS1-16954
September 1983

National Aeronautics and
Space Administration

Langley Research Center
Hampton, Virginia 23665

NASA Contractor Report 172228

Measurement and Analysis of Critical Crack Tip Processes Associated with Variable Amplitude Fatigue Crack Growth

S. J. Hudak, D. L. Davidson, and K. S. Chan
Southwest Research Institute
San Antonio, Texas

Contract NAS1-16954
September 1983

National Aeronautics and
Space Administration

Langley Research Center
Hampton, Virginia 23665

ABSTRACT

Crack growth retardation following overloads can result in overly conservative life predictions in structures subjected to variable amplitude fatigue loading when linear damage accumulation procedures are employed. Crack closure is believed to control the crack growth retardation, although the specific closure mechanism has been debatable. The current study provides new information on the relative contributions to crack closure from: 1) plasticity left in the wake of the advancing crack and 2) crack tip residual stresses. The delay period and corresponding crack growth rate transients following overloads are systematically measured as a function of load ratio (R) and overload magnitude. These responses are correlated in terms of the local "driving force" for crack growth as measured by crack tip opening loads and ΔK_{eff}. The latter measurements are obtained using a scanning electron microscope equipped with a cyclic loading stage; measurements are quantified using a relatively new stereo-imaging technique. Combining experimental results with analytical predictions suggests that both plastic wake and residual stress mechanism are operative, the latter becoming predominate as R increases. Additional critical experiments to further support this hypothesis are recommended.

TABLE OF CONTENTS

LIST OF FIGURES

LIST OF FIGURES (CONT.)

LIST OF TABLES

1.0 INTRODUCTION

Predicting the rate at which fatigue cracks will grow under variable amplitude loading is a major uncertainty in the design and reliability assurance of a variety of structures. Based on research over the last two decades, it is known that intermittent overloads, or high-low block loading sequences, can cause significant crack growth retardation relative to the steady state rate under constant amplitude loading [1-26]. The reverse effect, that is, accelerated growth due to underloads, or low-high loading sequences, is also known to occur; however, this phenomenon is much less pronounced than crack growth retardation [6-9]. Thus, in practice, it is primarily crack growth retardation which complicates the prediction of variable amplitude crack growth. Consequently, fatigue analyses which do not consider load interaction effects, but instead rely on linear damage accumulation, give conservative predictions, provided proper account is taken of all other factors. Depending on the nature of the load history and the operational requirements of the structure, this built-in conservatism may be intolerable--for example, aircraft and aerospace components where weight savings is a primary design goal.

Two distinctly different experimental approaches have been used to attack the variable amplitude fatigue crack growth problem. The first employs either random or highly-variable loading sequences in an attempt to represent typical spectra for specific components. This pragmatic approach is most often undertaken to solve specific design or reliability problems. While these results can be utilized as a test for an existing predictive model, they provide little insight into the physical processes involved in fatigue crack growth retardation.

The second approach employs relatively simple loading sequences--usually single or multiple overloads, or high-low block loading sequences. This more fundamental approach is designed to elucidate the process(es) by which crack growth retardation occurs, thereby providing critical tests for existing predictive models, as well as contributing to the development of improved models.

Based on the above approach, crack growth retardation has been shown to depend on a variety of variables, some of which interact in a complex manner. The influence of these variables is most often characterized in terms of the number of overload-affected cycles, often termed delay cycles, N_D. The value of N_D is most strongly influenced by the magnitude of the overload cycle. Specifically, increasing the magnitude of the overload cycle increases N_D [9-17]. Increasing the number of overload cycles also causes N_D to increase; however, this effect often saturates as the number of overload cycles increases [9-16]. Furthermore, the effect of a single overload can be significantly reduced when immediately followed by an underload [5, 16], although the application of an underload immediately preceding the overload has little or no influence on N_D [12].

Stress state influences N_D through several different test variables. For example, the larger plastic zone sizes associated with plane stress are believed to explain why N_D increases with decreasing specimen thickness [9, 14, 15, 19-23]. Alternatively, for a given thickness, the stress state will depend on the magnitude of K_{max}, or ΔK. Thus, stress state is believed to play a role in the observed increase in N_D as K_{max} is increased in certain alloys [9, 11, 19]. However, this effect appears to be complex since N_D has also been observed to decrease with increasing K_{max} in other alloys [5, 14, 21, 24]. Moreover, both trends have been observed in a single alloy, depending on the magnitude of the overload cycle [16]. Thus, the dependence of N_D on K_{max} appears to involve several underlying factors which have not yet been clearly elucidated. Similarly, the role of load ratio is also not clearly defined since only a few results exist on this variable and these are either conflicting [9, 11, 25] or confounded by simultaneous variations in other loading variables [26].

A commonly-held concept which has evolved in attempting to explain the above phenomenological results is that of an effective stress intensity factor which depends on the history of loading and thereby differs from the applied stress intensity factor obtained directly from remote loading. This local alteration of the "driving force" for crack growth has been postulated to result from a variety of processes--crack-tip blunting [4];

crack closure arising from residual compressive stresses developed ahead of the crack [3, 17, 29-31]; crack closure due to contact along the crack flanks arising from a plastically-deformed wake [9, 27, 28], oxide debris [32], or crack branching/asperity contact [32]. Alternatively, or perhaps supplementary, it has been suggested that overloads can alter the intrinsic material resistance to crack growth--specifically, by strain hardening material within the crack-tip overload plastic zone [33]. Although all of these processes undoubtedly occur during crack growth, the relative contribution of each to the retardation phenomenon remains unknown. Indeed, it may not be possible to completely isolate the contribution of each of these processes since many are inextricably related through the plastic deformation attending crack growth.

Several semiempirical, engineering models have evolved in an attempt to predict crack growth retardation [34-38]. Although these models are based on the concept of an effective crack-tip stress intensity factor, they do not explicitly treat those physical processes thought to contribute to crack growth retardation. Nevertheless, they have proven to be useful engineering tools, provided their empirical constants are determined for loading spectra which are similar to service spectra. However, they are known to break down for several ordered spectra; thus, their general applicability is uncertain.

Recently, more fundamental analyses of crack closure have been undertaken. Two-dimensional, elastic-plastic finite element analyses have been shown to qualitatively explain many of the phenomena observed during both constant amplitude crack growth and simple overload histories [39-43]. However, these analyses are too costly to apply on a cycle-by-cycle basis to predict crack growth under typical service spectra. Thus, simpler models of crack closure have been pursued [44-51] based on extensions of Dugdale's strip yielding approach [52]. However, these idealized analyses need further evaluation to determine whether they contain sufficient detail to adequately describe those processes which contribute to crack closure and crack growth retardation.

The primary objective of this study was to better define the relative contributions to crack closure of 1) residual stress ahead of the crack-tip, and 2) plastically-deformed wake along the crack flanks. The approach taken is to measure N_D and corresponding crack-tip opening loads (P_{op}) resulting from single overloads while systematically varying load ratio (R = 0.1, 0.33, 0.5) and overload magnitude. Measurements of P_{op} are obtained using a scanning electron microscope (SEM) equipped with a hydraulic loading stage. This relatively new tool has proven to be useful in acquiring mechanistic information on fatigue crack propagation under variable amplitude loading [29-31]. Simplified models of crack closure based on residual stress and plastically-deformed wake are used to assist in interpretation of results and formulation of additional critical experiments.

The views and conclusions presented in this report reflect solely the authors' opinions. Use of commercial products or names of manufacturers in this report does not constitute official endorsement of such products or manufacturers, either expressed or implied, by the National Aeronautics and Space Administration.

2.0 DEFINITION OF TERMS

Phenomenological studies of crack growth retardation following single overloads have employed several different definitions for the magnitude of the overload, as well as the resulting number of delay cycles. These differences need to be recognized when interpreting and comparing data from several sources.

In order to define the magnitude of the overload, consider the loading spectrum given in Figure 1 and the associated extreme values and ranges of the crack-tip stress intensity factor. Experiments are commonly conducted so that the mean stress of the baseline cycling is maintained constant during a given overload test by fixing the load ratio ($R = K_{min}/K_{max} = P_{min}/P_{max}$). The definition of the overload ratio can be formulated in terms of the ratio of either the maximum values or ranges of the stress intensity factor for the overload to base loading cycles giving either

$$OLR = K_{OL}/K_{max} = P_{OL}/P_{max} \tag{1}$$

$$OLR^* = \Delta K_{OL}/\Delta K = (P_{OL} - P_{min})/(P_{max} - P_{min}) \tag{2}$$

where P_{min} and P_{max} are the minimum and maximum load values in the base cycle, and P_{OL} is the maximum load in the overload cycle. As indicated in Equations 1 and 2, OLR is referenced to zero load, while OLR* is referenced to the minimum load in the history. Thus, both definitions are identical when $P_{min} = 0$ ($R = 0$). However, in general the relationship between OLR and OLR* depends on K as follows:

$$OLR^* = \frac{OLR - R}{1 - R} \tag{3}$$

The current study uses either OLR and OLR* depending upon which is most suitable to illustrate a given point; for example, OLR is used for

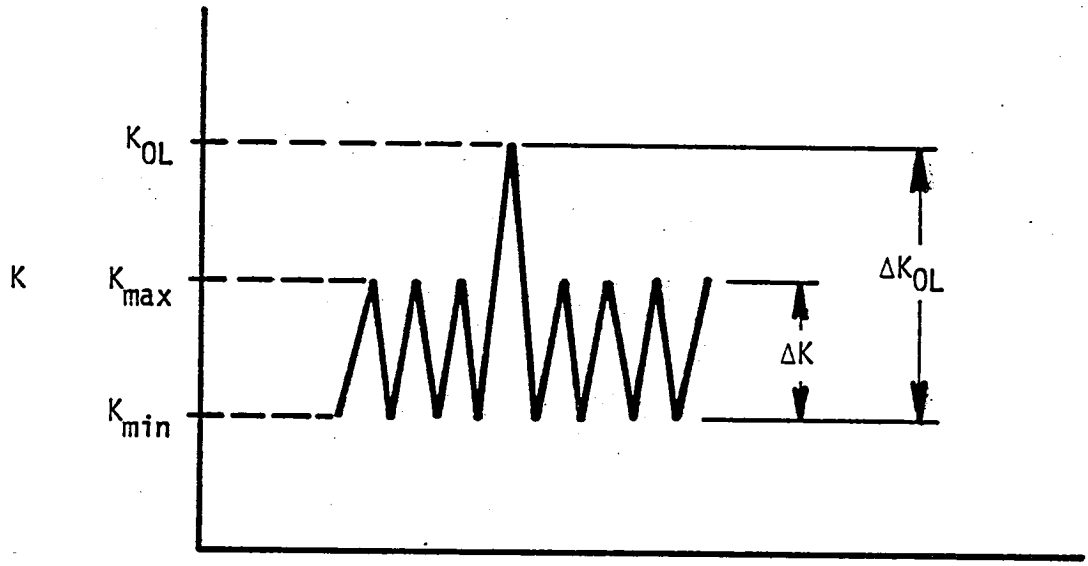

$$R = K_{min}/K_{max} = P_{min}/P_{max}$$

$$OLR = K_{OL}/K_{max} = P_{OL}/P_{max}$$

$$OLR^* = \Delta K_{OL}/\Delta K = (P_{OL} - P_{min})/(P_{max} - P_{min})$$

$$OLR^* = \frac{OLR - R}{1 - R}.$$

FIGURE 1. CHARACTERIZATION OF LOAD-HISTORY AND DEFINITIONS OF OVERLOAD MAGNITUDE

convenience when comparing results from various studies since this measure has been most frequently used in the past. However, OLR* is used to compare results at different R values since it provides a more meaningful measure of the overload magnitude when mean stress is varied.

The various definitions which have been used for the number of delay cycles are illustrated in Figure 2. The typical response of crack length versus number of cycles and corresponding crack growth rate versus number of cycles are shown in Figures 2(a) and 2(b), respectively. The response of the crack during a single overload experiment is as follows. Initially, steady state crack growth occurs in region a-b at stress intensity factor ΔK_1 immediately preceding the overload. The overload cycle corresponding to ΔK_{OL} then causes a brief accelerated growth period in region b-c, followed by a precipitous decrease in growth rate to a minimum growth rate and eventual recovery in region c-e. Steady state growth is reestablished in region e-f at ΔK_2. Generally, ΔK_2 is nearly equal to ΔK_1 since growth has only occurred over a crack length interval which is on the order of the plastic zone size of the overload. In certain instances, ΔK during the above sequence is maintained more nearly constant by applying step decreases in load as the crack grows.

Jonas and Wei [5] have proposed that delay be operationally defined in terms of a period over which the effective crack growth is zero by constructing c-d and e-d to give N_D' as shown in Figure 2(a). Alternatively, several investigators (for example, References 16, 24, and 25) have simply defined delay as the number of cycles over which the crack growth rate is less than the preoverload value--this measure corresponds to b-e in Figures 2(a) and 2(b) and is labeled N_D.

The above two definitions can differ significantly, particularly for low overload ratios where the delay period is relatively small. Also note that N_D will always be greater than N_D' since the latter is based on the extrapolation e-d and, in addition, does not include the accelerated growth period b-c.

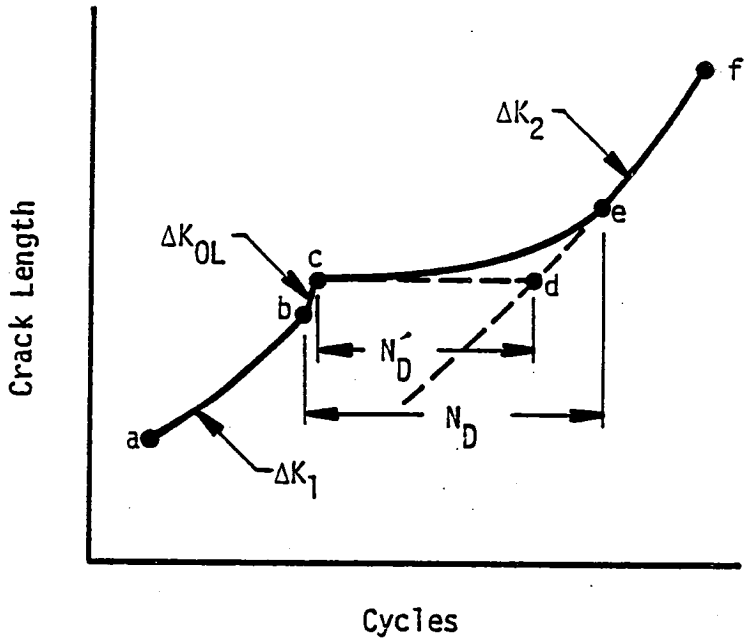

(a) Delay Cycles Defined Using Crack Length Versus Elapsed Cycles Data

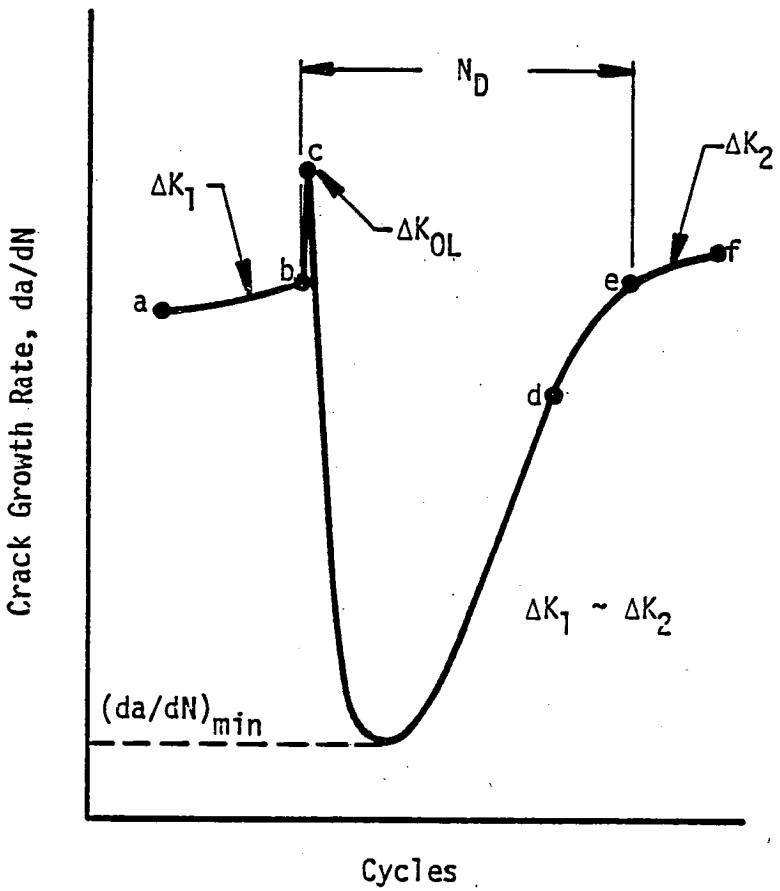

(b) Delay Cycles Defined Using Crack Growth Rate Data

FIGURE 2. OPERATIONAL DEFINITIONS OF NUMBER OF DELAY CYCLES FOLLOWING A SINGLE OVERLOAD

The current study uses N_D as the measure of delay primarily because it is a relatively straightforward operational definition which can be easily applied to both experimental data and model predictions merely by monitoring the postoverload growth rate. On the other hand, N_D' requires a cumbersome geometric construction and is somewhat artificially defined.

3.0 APPROACH

3.1 Material

The material selected for study was X7091-T7E69 aluminum*, a relatively new aerospace alloy produced using powder metallurgy (P/M) technology. This process results in a microstructure and composition which is more homogeneous than those of conventional cast ingot metallurgy (I/M) practices [53, 54]. Alloy X7091 was selected for study for several reasons. First, its fine-grain size (approximately 5 μm) should result in relatively homogeneous deformation thereby producing results which are less sensitive to microstructural variations than are results on comparable I/M alloys. Thus, the problem of determining average values of microscopically-measured crack opening loads from a relatively few number of measurements is minimized. Secondly, it is of interest to compare the crack growth retardation behavior of this relatively unstudied P/M alloy with the many results available on I/M alloys.

The alloy was obtained from the Aluminum Company of America in the form of an extruded bar (38 x 114 x 610 mm) in the T7E69 condition which included a stress relief treatment by stretching. The nominal chemical composition of this alloy is given in Table I. Both monotonic and cyclic stress-strain properties which we measured are provided in Table II. For comparison, the monotonic properties reported by Alcoa as being typical for this alloy are also provided in Table II and indicate that the material used herein is representative of commercial products.

The measured monotonic and cyclic stress-strain responses indicate that X7091-T7E69 is cyclically stable as illustrated from the true stress versus true plastic strain curves for both loading conditions given in

---

* Prior to mid-1980, this alloy was designated MA87 during original laboratory development and subsequently renamed CT91 as limited quantities became available for customer evaluation.

TABLE I

CHEMICAL COMPOSITION LIMITS FOR P/M ALUMINUM ALLOY X7091

Weight Percent								
Si	Fe	Cu	Mg	Zn	Co	O	Others	Al
0.12	0.15	1.1 - 1.8	2.0 - 3.0	5.8 - 7.1	0.20 - 0.60	0.20 - 0.50	0.15	Balance

TABLE II

ROOM TEMPERATURE MECHANICAL PROPERTIES* FOR P/M ALUMINUM ALLOY X7091

Source	Loading	Yield Strength (MPa)	Ultimate Strength (MPa)	Elongation (%)	Strain Hardening Exponent	K_{Ic} (MPa$\sqrt{m}$)
Alcoa	Monotonic	517	565	13	-	30
This STudy	Monotonic	553	602	11	0.058	-
This Study	Cyclic		-	-	0.071	-

* All tensile and fatigue properties measured in the longitudinal direction; fracture toughness measured in the transverse (L-T) direction.

Figure 3. The stress versus total strain responses are represented by the following equations:*

Monotonic Loading:

$$\varepsilon = \frac{\sigma}{E} + \left(\frac{\sigma}{730}\right)^{1/0.058} \tag{4}$$

Cyclic Loading:

$$\Delta\varepsilon/2 = \frac{\Delta\sigma/2}{E} + \left(\frac{\Delta\sigma/2}{785}\right)^{1/0.071} \tag{5}$$

where E = 72,800 MPa, the elastic modulus.

Constant amplitude fatigue crack growth rate data on X7091 at R = 0.33 and 0.8 are available from Reference 55 and are provided in Figure 4. Data at R = 0.33 from three different extrusions, including average preoverload measurements from the current study, indicate that these properties do not vary markedly from extrusion-to-extrusion. Thus, it is reasonable to use the average growth rate behavior from data in Figure 4 to derive the crack growth constants needed for use with the closure model described in Section 5.2.

3.2 Specimen Design and Preparation

All experiments were performed using the 3.0-mm-thick, single-edge-notched specimen shown in Figure 5. Specimens were machined from the extrusion so that cracks could be propagated transverse to the primary forming direction--that is, in the L-T orientation.

The stress intensity factor calibration for this specimen is given in Reference 56.

Fatigue loading of the specimen was accomplished by pin loading--the central holes were employed when using a conventional servo-hydraulic fatigue machine, and the four edge-notches were employed when using the SEM

---

* Equations are for units in MPa.

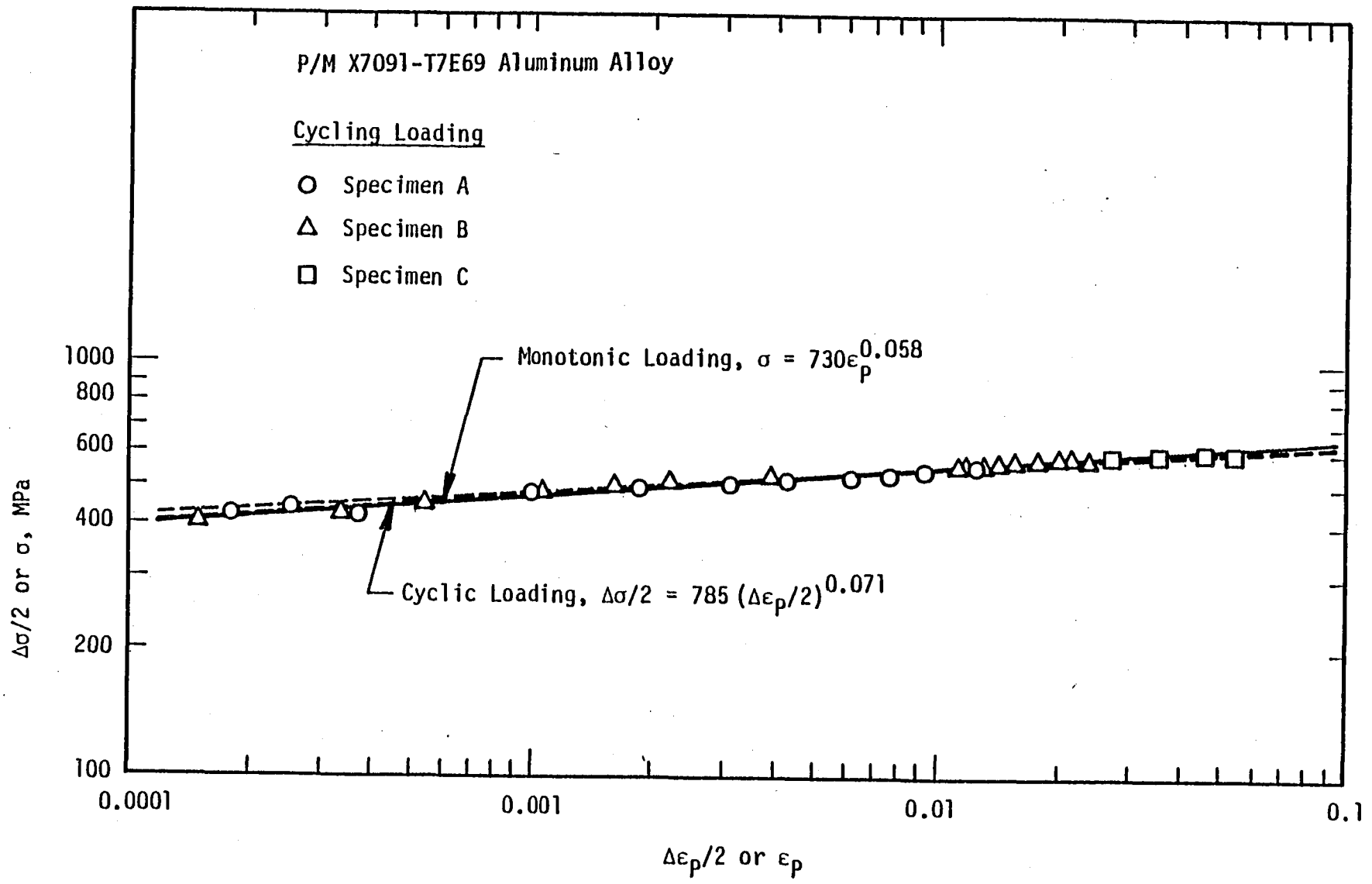

FIGURE 3. STRESS VERSUS PLASTIC STRAIN RELATIONS FOR CYCLIC AND MONOTONIC LOADING IN P/M ALUMINUM ALLOY X7091-T7E69.

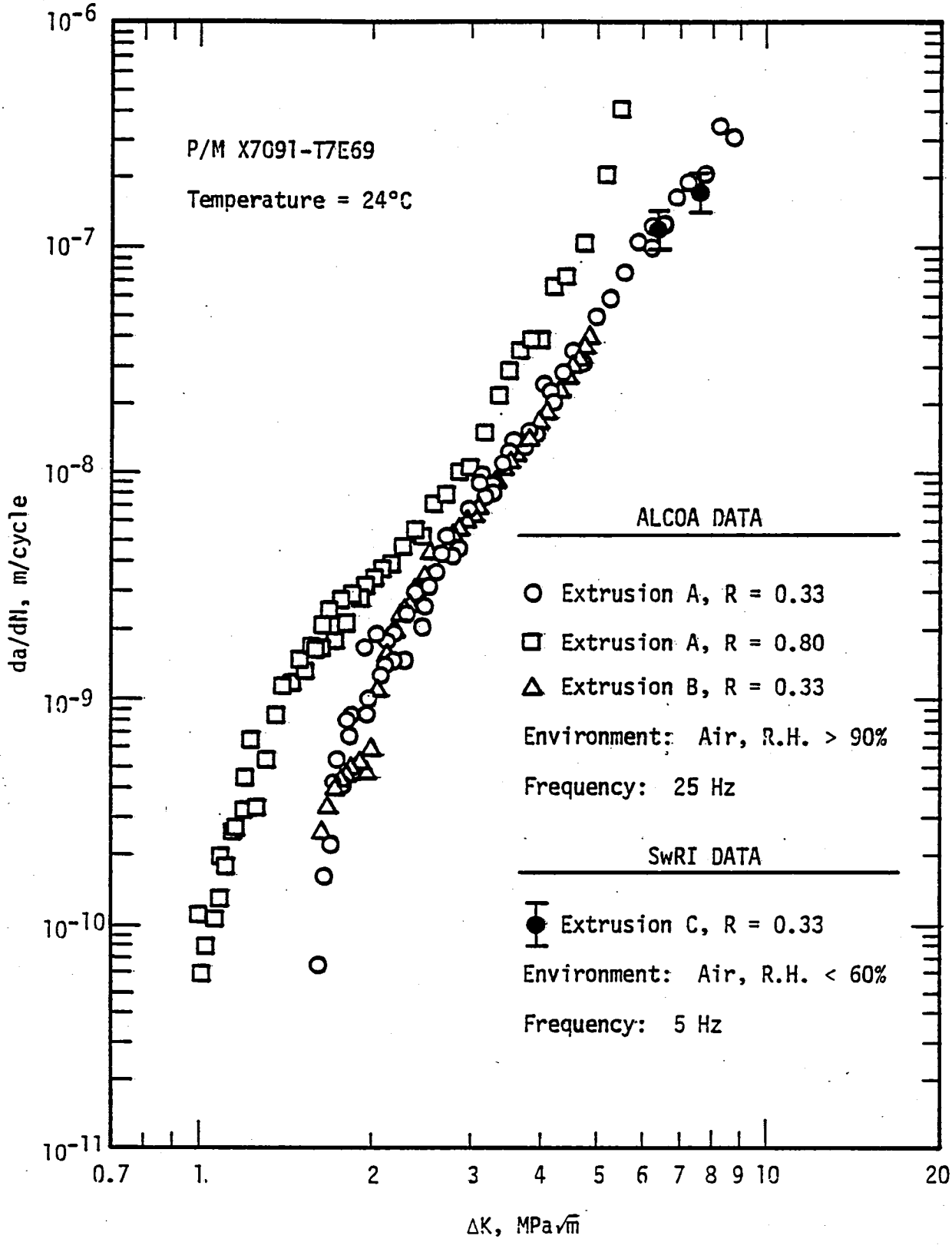

FIGURE 4. COMPARISON OF FATIGUE CRACK GROWTH RATE BEHAVIOR FROM SEVERAL PRODUCTION EXTRUSIONS OF P/M ALUMINUM ALLOY X7091-T7E69

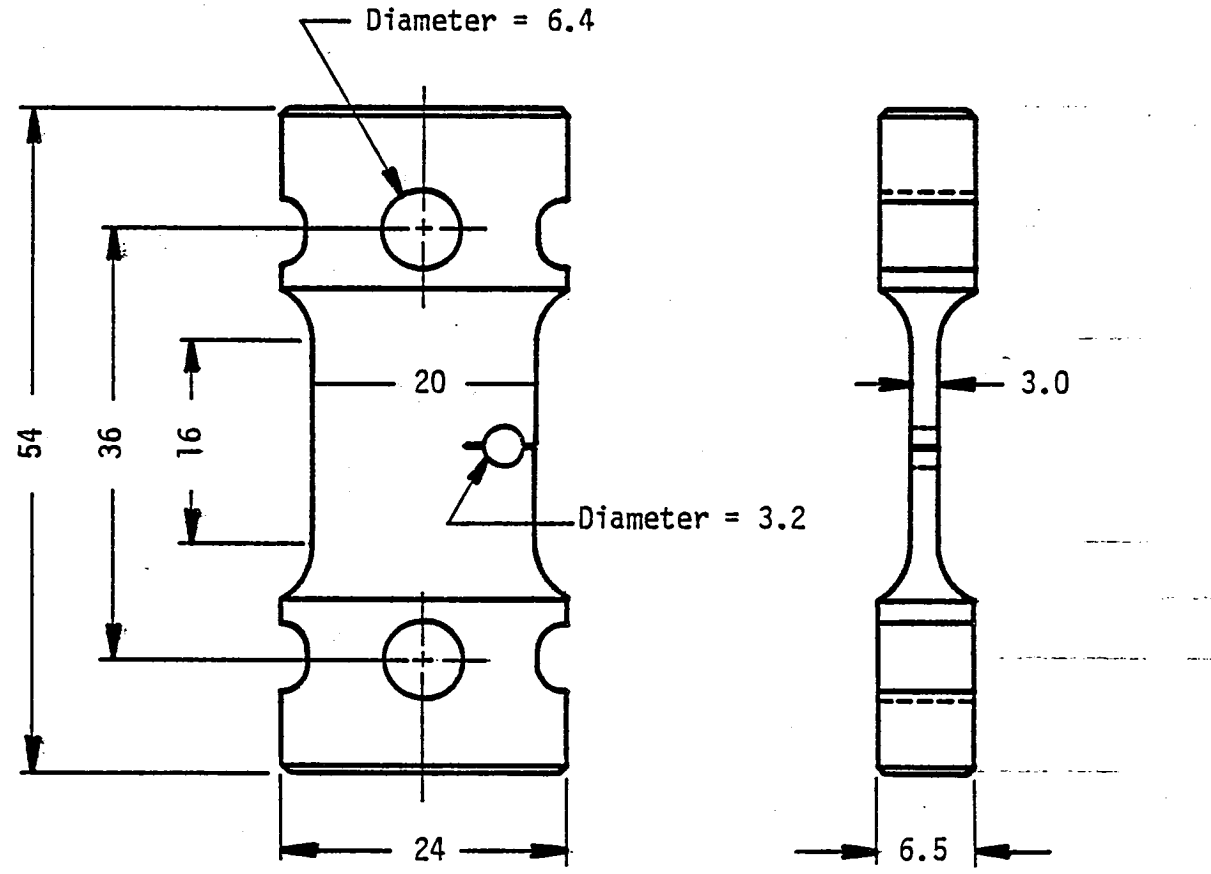

FIGURE 5. SINGLE-EDGE-NOTCHED SPECIMEN USED IN OVERLOAD EXPERIMENTS. Split-pin is used to apply wedge force to 3.2-mm hole, thereby maintaining mean stress when transferring specimen from test machine to SEM loading stage.

loading stage. The 3.2-mm-diameter hole at the midgage-length of the specimen was designed to accommodate tapered, split pins which were used to apply a wedge force to the crack. This system was employed whenever the specimens were removed from the conventional fatigue machine for various measurements, as described in the following section.

The specimen gage section was metallographically polished and etched, primarily to enhance the resolution of the SEM measurements. The etching solution contained 25% HNO_3 and 75% CH_3OH and was applied to the specimen for about one minute.

In initial experiments, specimens were mechanically-polished using the following sequency: 240-, 400-, 600-grit paper; 6-μm, 1-μm, and 0.3-μm diamond paste; 0.05-μm alumina polishing compound. After several experiments, it was determined that this procedure resulted in a damaged surface layer, either from the mechanical polishing procedure or from the residual effects of machining. This surface layer resulted in a multitude of fine surface cracks, many of which exhibited unusual crack-tip opening responses under load. This anomalous surface behavior was eliminated by electropolishing after mechanical polishing down to the 1 μm finish.

3.3 Measurement Technique

During the course of each overload experiment, crack growth was monitored on the specimen surface using a 530X optical microscope equipped with a precision measurement stage. These measurements were made by periodically removing the specimen from the fatigue machine, during which time a mean load (approximately equal to the mean test load) was applied to the specimen using the previously-described wedge loading technique. This technique served to preclude underloading the specimen in the high R tests, as well as to enhance the resolution of the crack tip during crack length measurements in the optical microscope. With this procedure, the crack length measurement accuracy is estimated to be ± 0.01 mm. Crack growth rates were computed from these data using the secant, or point-to-point, method over crack length intervals of no less than 0.05 mm.

Specimens were periodically transferred to the SEM for more detailed measurements; again, wedge loading was employed to prevent underloading during the transfer. Overload cycles were applied while in the SEM using a specially-designed, hydraulically-actuated loading stage [57]. This system enabled direct measurement of crack-tip opening loads before and after the overload as well as a high resolution view of the crack extension process [29-31].

Crack opening loads were determined in the SEM loading stage by using the stereoimaging technique [58] and the following procedure:

(1) The crack-tip region was photographed at minimum load.

(2) Load was slowly applied until the crack tip appeared to initially open; a second photograph was made at this point.

(3) Photographs from (1) and (2) were compared using a stereoviewer. (With this stereographic procedure, any opening at the crack tip appears as an out-of-plane displacement.) If the crack tip appeared closed, another photograph was taken at a slightly higher load and compared with (1).

(4) If the crack tip appeared open, the specimen was unloaded, then reloaded to a lower load; another photograph was taken and compared with (1). Procedures (3) and (4) were repeated until P_{op} was established.

Although the above iterative procedure is relatively time consuming, it produces a direct and very accurate determination of the crack-tip opening load. Measurements on cracks of different lengths, but under nominally identical loading conditions, exhibit variations of ± 25% in crack opening load. Although the measurement precision of the technique has not been rigorously established, it is believed that it is significantly less than the above variability, thereby suggesting that these variations arise from the inherent randomness of the fatigue process on this size scale.

SEM photographs were also obtained at minimum and maximum load periodically throughout the overload experiments; application of stereo-imaging to these measurements is planned in a future study in order to determine the crack-tip stress-strain fields during overloads [59].

4.0 EXPERIMENTAL RESULTS AND DISCUSSION

4.1 Opening Loads and ΔK_{eff} During Constant Amplitude Crack Growth

Measured crack-tip opening loads, P_{op}, for constant amplitude fatigue crack growth at load ratios of 0.1, 0.33, and 0.5 are given in Figure 6. Here values of P_{op} have been normalized by P_{max}. The dashed line, inclined at 45°, represents $P_{op} = P_{min}$--that is, the ideal case where no closure occurs. Therefore, deviations between the measured P_{op}/P_{max} values and the line $P_{op} = P_{min}$ reflect the extent of crack closure.

The above measurements can also be expressed in terms of an effective stress intensity factor range, ΔK_{eff}, by means of the following relationship.

$$\frac{\Delta K_{eff}}{\Delta K} = \frac{P_{max} - P_{op}}{P_{max} - P_{min}} = \frac{1 - P_{op}/P_{max}}{1 - R} \quad . \qquad (6)$$

Results in Figure 7 were obtained from applying Equation 6 to the data in Figure 6. As indicated, ΔK_{eff} increases from 45% to 64% of ΔK as R increases from 0.1 to 0.5. Previous data of Lankford and Davidson [31] on several I/M aluminum alloys are also provided in Figure 7 for comparison. Although these results are in reasonable agreement with those on P/M Alloy X7091-T7E69, they do suggest a decrease in ΔK_{eff} with increasing alloy strength level.

Also given in Figures 6 and 7 are the predicted ΔK_{eff} values from crack closure models based on the concepts of a plastically-deformed wake and of crack-tip residual stress; these models are discussed in subsequent sections.

4.2 Delay Cycles

Turning now to the measurements of N_D as a function of the magnitude of the overload, first consider Figure 8, where results on the P/M Alloy

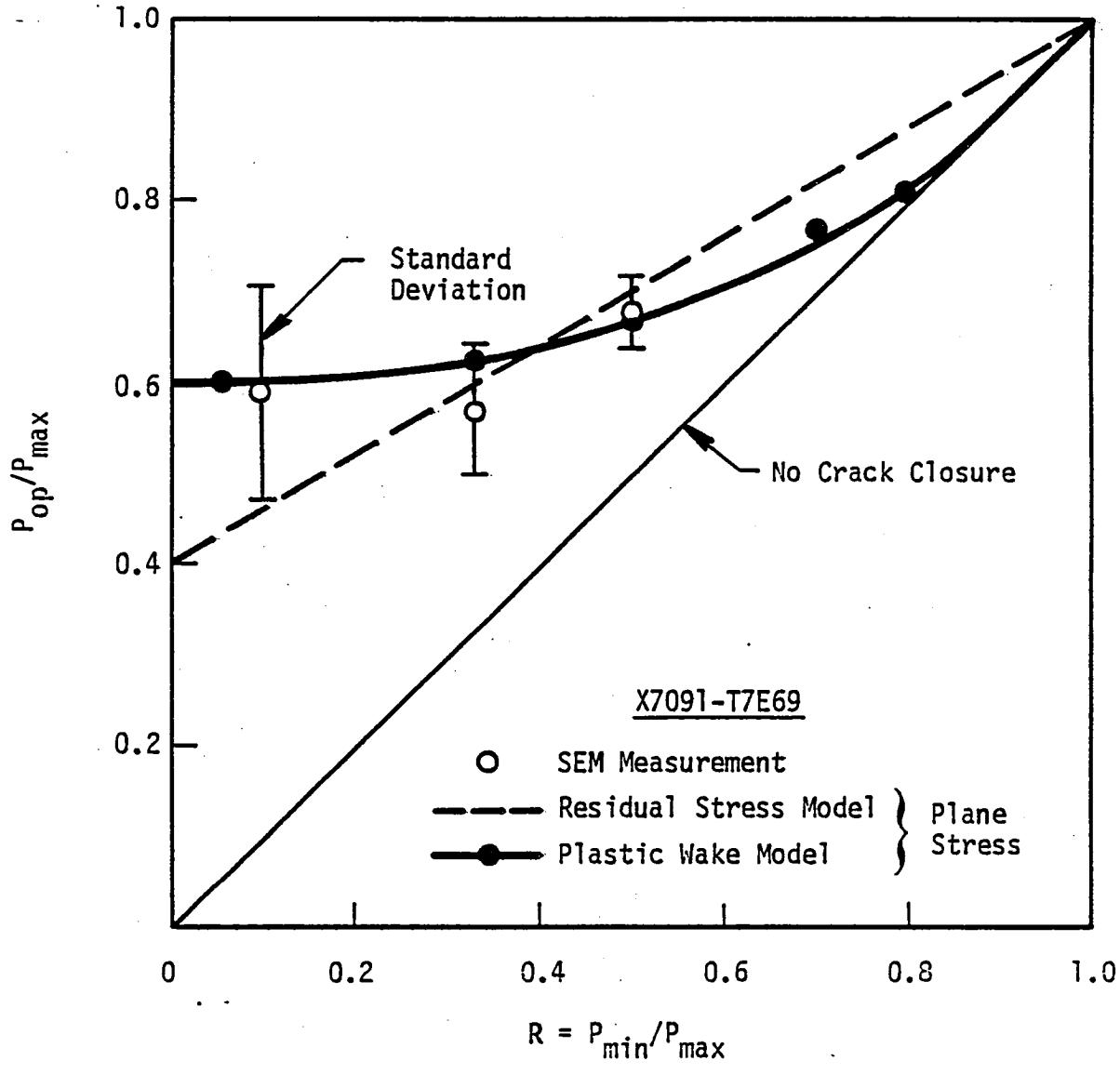

FIGURE 6. COMPARISON OF MEASURED AND PREDICTED CRACK OPENING LOAD (P_{op}) AS A FUNCTION OF LOAD RATIO (R) FOR CONSTANT AMPLITUDE FATIGUE CRACK GROWTH

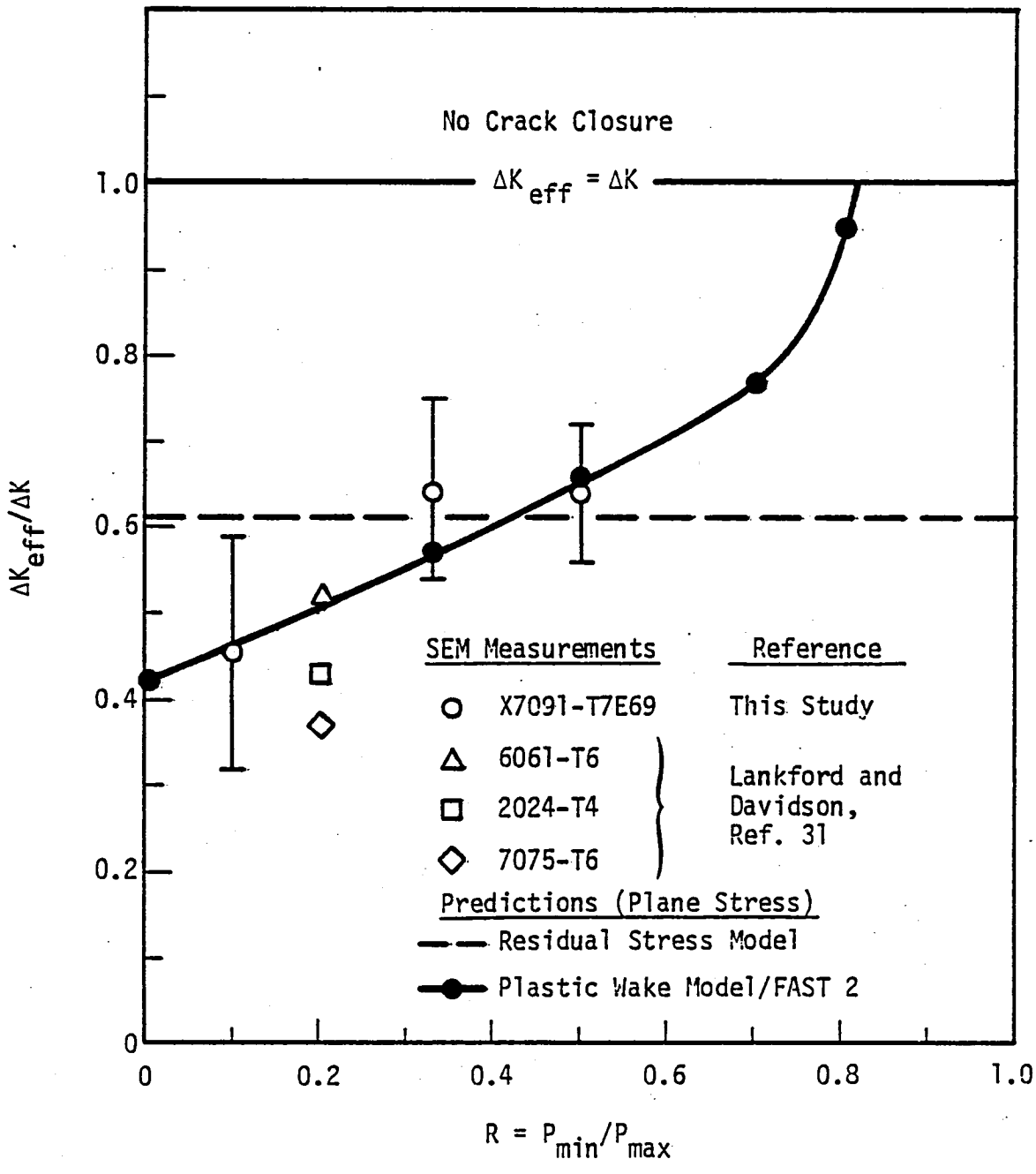

FIGURE 7. COMPARISON OF MEASURED AND PREDICTED EFFECTIVE CRACK-TIP STRESS INTENSITY RANGES (ΔK_{eff}) AS A FUNCTION OF LOAD RATIO (R) FOR CONSTANT-AMPLITUDE FATIGUE CRACK GROWTH

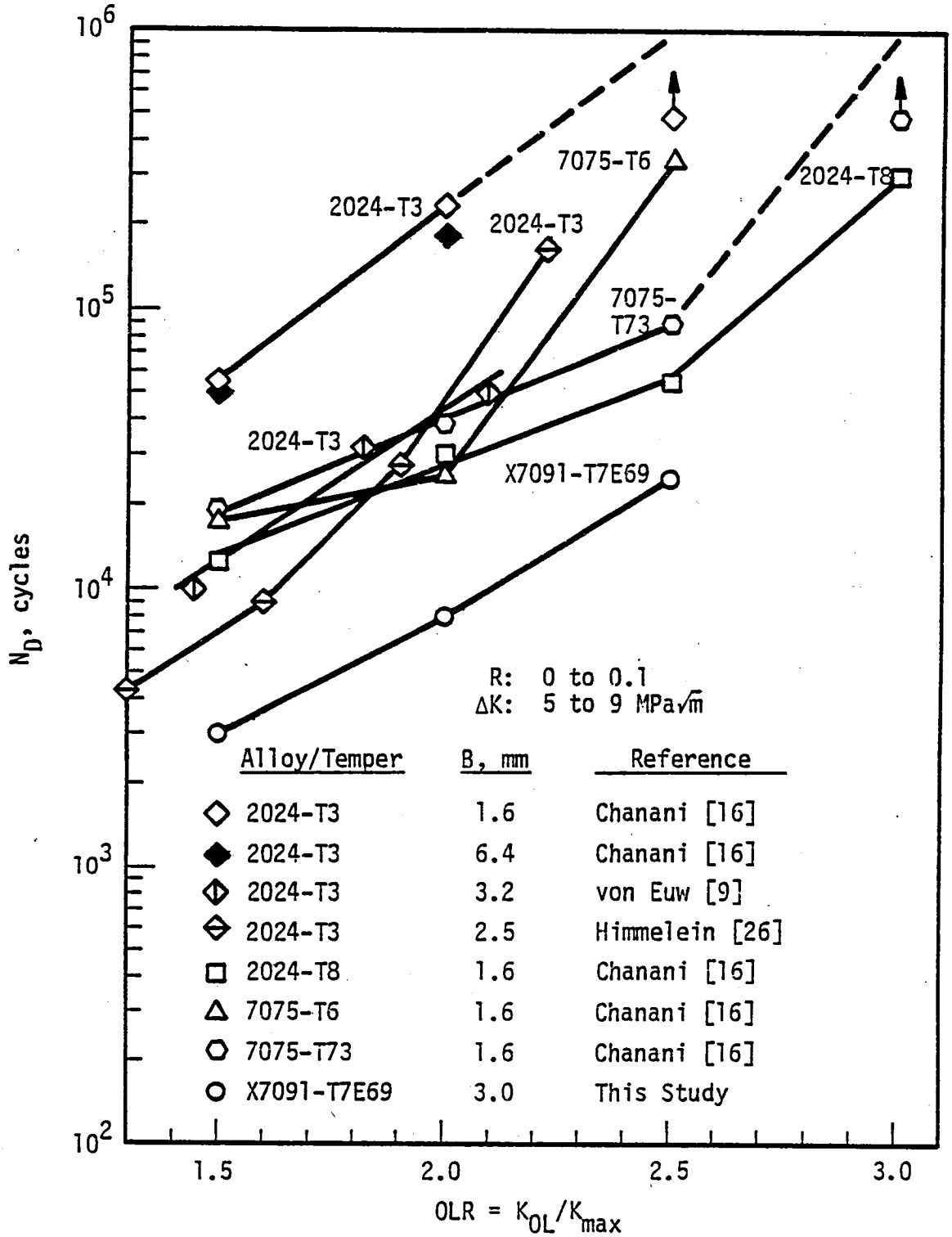

FIGURE 8. COMPARISON OF DELAY CHARACTERISTICS OF P/M ALUMINUM ALLOY X7091-T7E69 WITH THOSE OF COMMON I/M ALUMINUM ALLOYS

X7091-T7E69 are compared with literature data on a variety of I/M alloys. Interestingly, results show X7091-T7E69 to exhibit less delay at a given value of OLR than any of the other I/M alloys. Specimen thickness for each of the materials is also listed in Figure 8 to illustrate that these differences cannot be attributable to the known trend of increasing N_D with decreasing thickness.

The data in Figure 8 on 2024-T3 also indicate the amount of variation in N_D that can be expected from plate-to-plate. Once again, these differences do not appear to be due to variations of specimen thickness since Chanani's data [22] indicate very little effect of this variable, at least in the plate he examined.

The delay characteristics of P/M Alloy X7091-T7E69 as a function of load ratio are given in Figure 9. As indicated in Section 2.0, these results are best expressed in terms of OLR*. The measured results at R = 0.33 and R = 0.50 are not measurably different, while those at R = 0.1 appear to give longer delay periods for a given value of OLR*. Limited data of von Euw et al [9] at OLR* = 2.0 and Trebules et al [11] at OLR* = 1.5 tend to support this trend for 2024-T3, while those of von Euw et al [9] at OLR = 1.5 indicate little effect of R on N_D. Brown and Weertman [25] have also indicated that increasing R from 0.05 to 0.5 has no effect on N_D at OLR* = 1.8 in 7050-T76 aluminum.

4.3 SEM Micrographs of Overload Sequences

Before considering the influence of single overloads on the retardation of growth rates and on corresponding P_{op} levels, let us first examine SEM micrographs showing crack paths and crack-tip opening displacements for several interesting overload sequences. These photographs provide qualitative information on how cracks respond to overloads and demonstrate the scale at which measurements were made.

Figures 10 through 12 show the overall crack path and crack openings during selected points in the overload experiments at OLR = 2. Notice that the crack paths exhibit a similar trend in all cases. Specifically, prior to the overload, crack growth is predominantly normal to the direction of

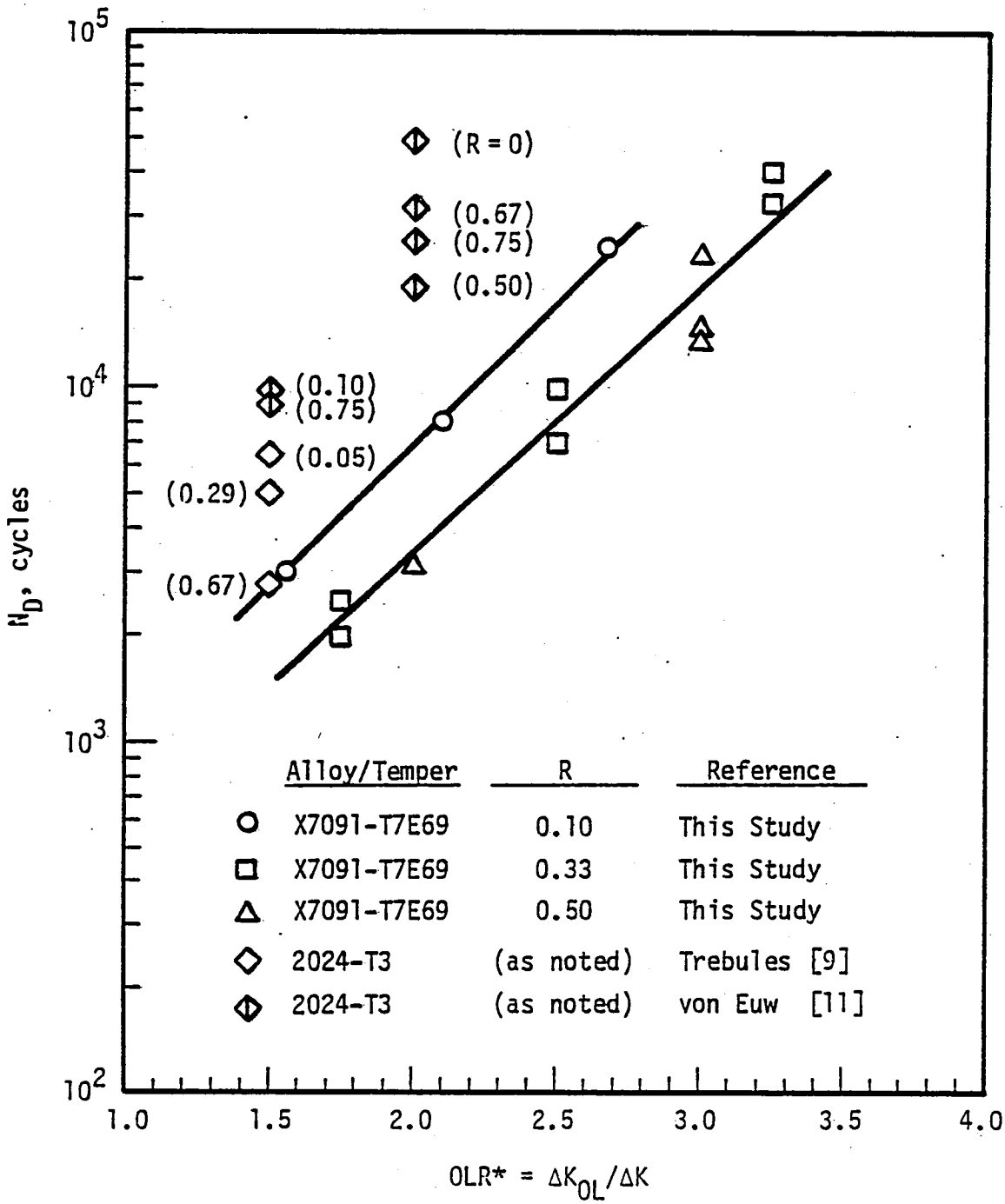

FIGURE 9. DELAY CHARACTERISTICS OF P/M ALLOY X7091-T7E69 AND I/M ALLOY 2024-T3 FOR VARIOUS LOAD RATIOS

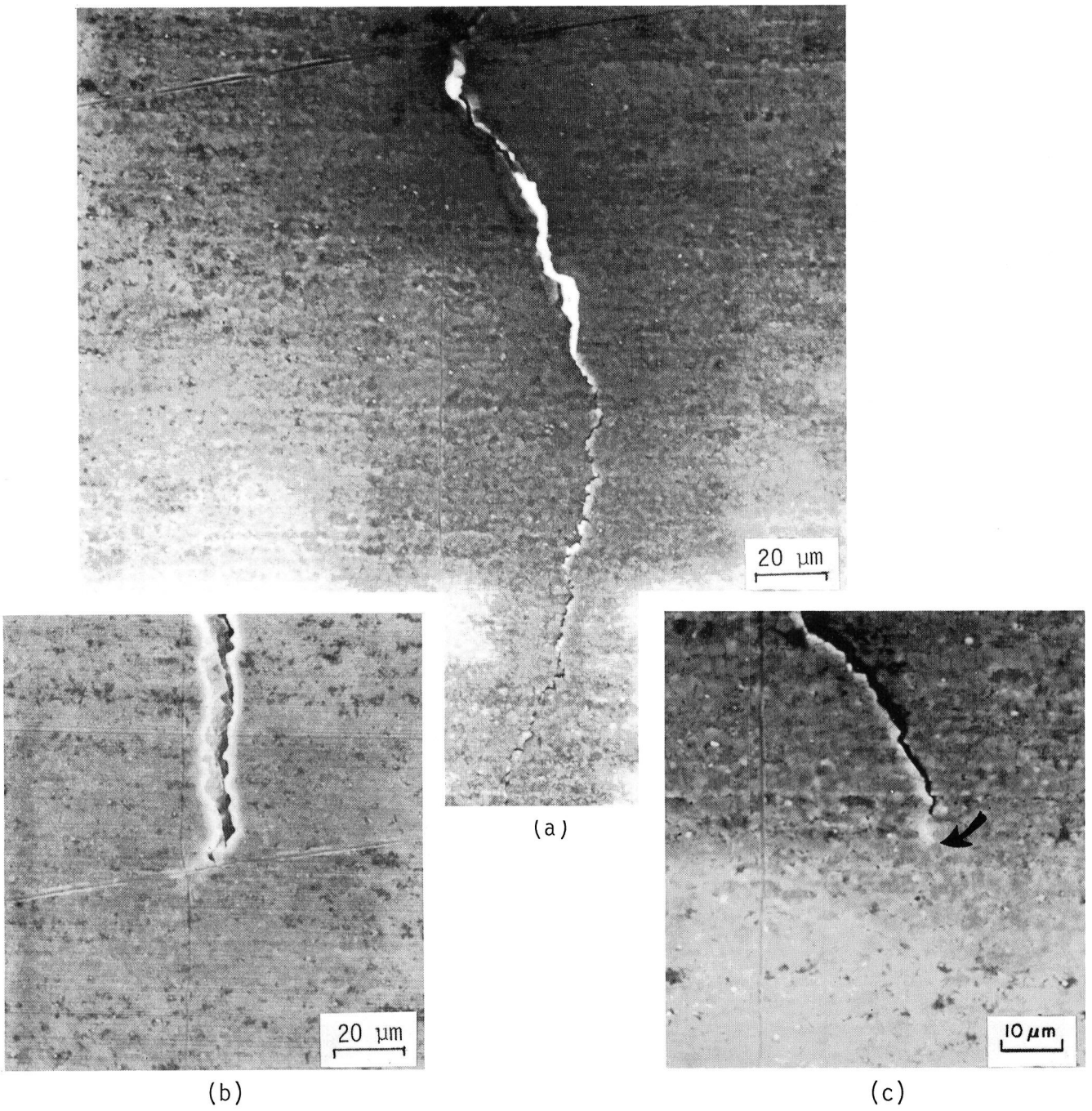

FIGURE 10. SEM MICROGRAPHS SHOWING CRACK GROWTH PATH AND SELECTED CRACK-TIP OPENINGS FOLLOWING A SINGLE OVERLOAD AT OLR=2, R=0.16: (a) overall crack path; (b) crack opening at maximum load in the overload cycle; (c) crack opening near the minimum rate of crack growth following the overload. Arrow marks crack tip.

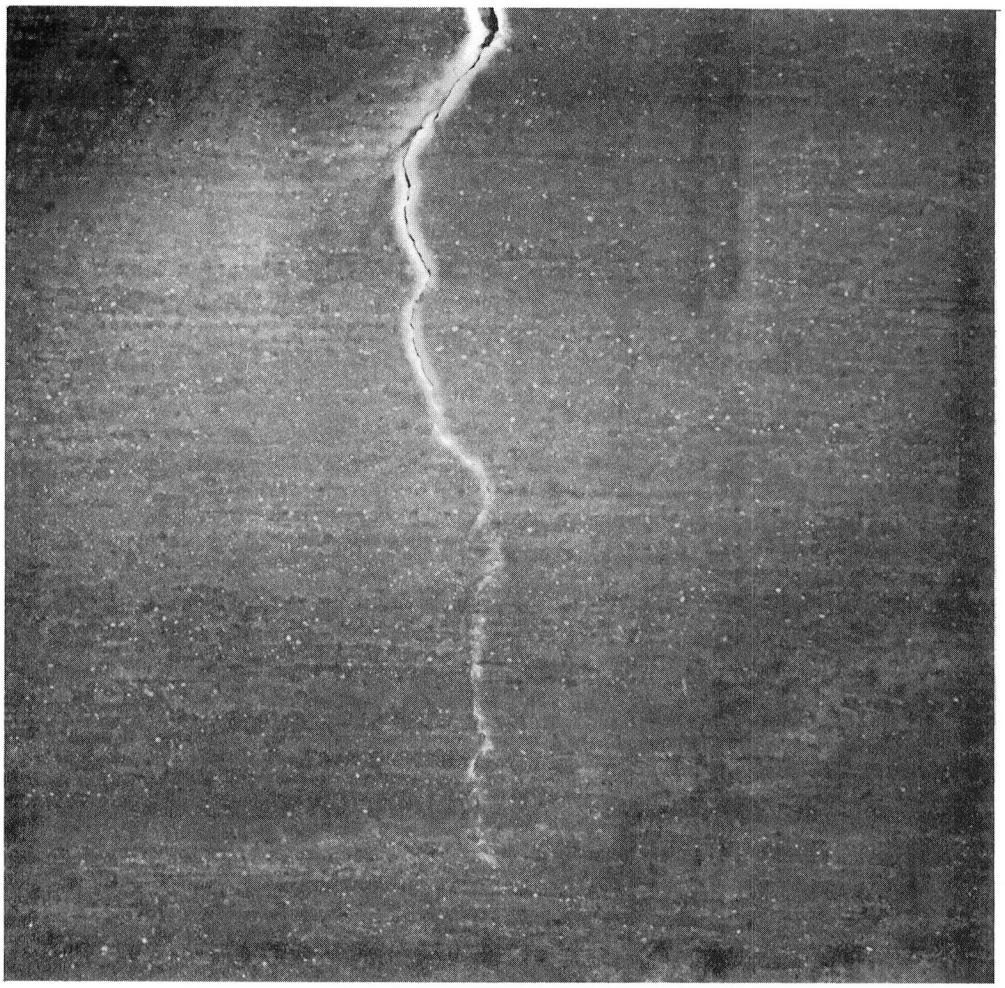

(a)

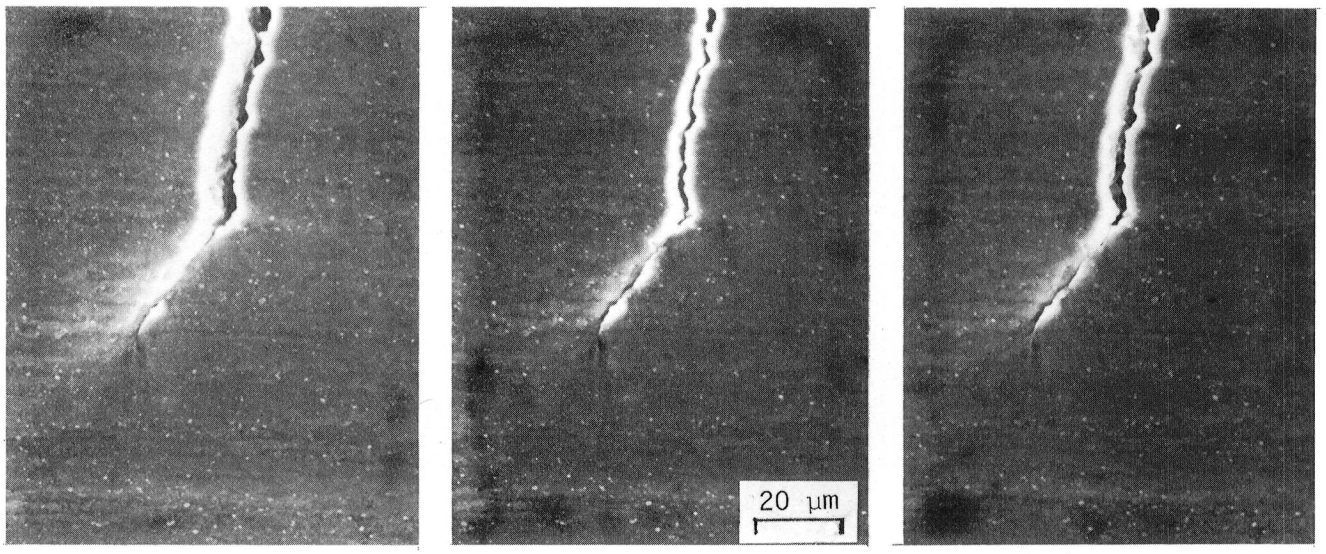

(b) (c) (d)

FIGURE 11. SEM MICROGRAPHS SHOWING CRACK GROWTH PATH AND SELECTED CRACK-TIP OPENINGS FOLLOWING A COMPLETELY REVERSED OVERLOAD/UNDERLOAD CYCLE AT OLR=2, R=0.5 (all photographs have same magnification): (a) overall crack path; (b) crack opening at minimum cyclic load following the overload; (c) crack opening at the reduced load (near zero) of the underload; (d) crack opening at minimum cyclic load following the underload.

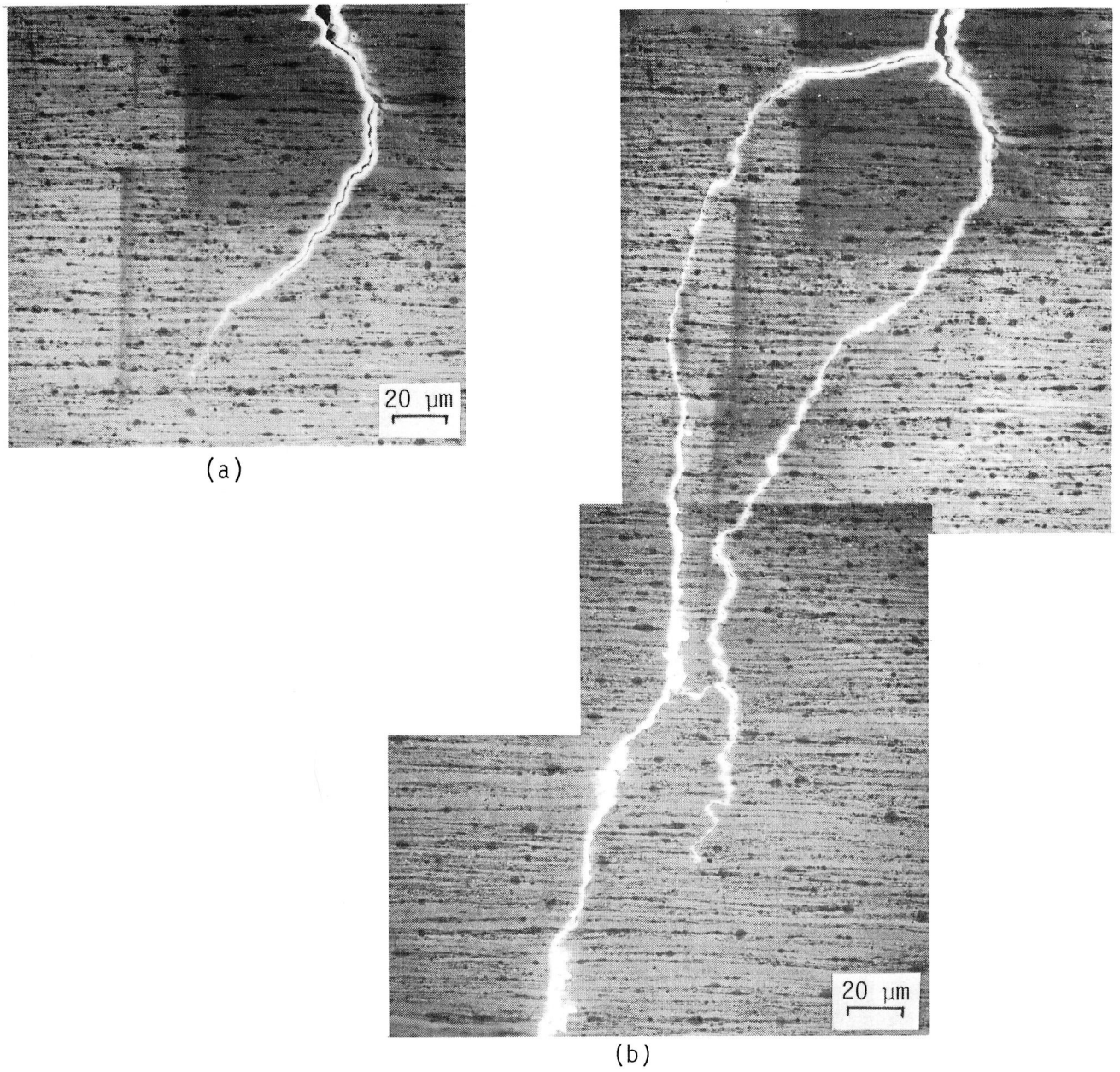

FIGURE 12. SEM MICROGRAPHS SHOWING THE CRACK PATH FOLLOWING AN OVERLOAD AT OLR=2, R=0.5: (a) near the minimum growth rate at 5650 cycles after the overload; (b) at 14,750 cycles after the overload, showing the formation of a second crack.

applied loading. In contrast, crack growth during and immediately following the overload is inclined at an angle of about 45° to the loading direction [Figures 10(a), 11(a), and 12(a)]. This initial growth direction coincides with intense shear band formation along these directions, as has been noted previously for a variety of aluminum alloys [29-31]. Although two relatively symmetric shear bands occur at the crack tip, subsequent crack growth usually follows one or the other of these bands. However, in certain cases, predominantly at high load ratio where the value of K_{OL} approaches K_{Ic}, a second crack will form along the second shear band as indicated in Figure 12(b). Generally, this second crack forms and grows very rapidly while the original crack becomes dormant, thereby enabling the second crack to join and/or sometimes outgrow the first crack.

The crack-tip opening displacements can vary greatly during the course of the overload experiment. For example, compare the large opening during the overload cycle, Figure 10(b), with that during the period of minimum crack growth rate ($< 10^{-9}$ m/cycle) following the overload, Figure 10(c). In fact, in the latter case, it is significant to note that the crack tip remains virtually closed, even at the maximum load in the cycle.*

Figure 11 illustrates the response of the crack when an overload is followed by an underload to zero load. Figure 11(b) shows the crack tip at minimum load following the overload, but prior to application of the underload, while Figure 11(c) shows the crack at near-zero load during the underload. The latter results in a significant decrease in overall crack opening and crushing of the crack surfaces in the region of the crack tip. Using the crack surface asperities as references, Figures 10(b) and 10(c) can be compared to show that this process occurs by combined Mode I/Mode II crack face displacements. In Figure 11(d), the crack is once again at the minimum load of the baseline cycling. However, notice that the crack opening is less than that exhibited at this load before the underload.

---

* The dark region along the crack in Figure 10(c) is not crack opening, but rather material, probably oxides, being extruded from the crack.

4.4 Crack Growth Response and ΔK_{eff} Following Overloads

Figures 13 through 15 give the measured ΔK_{eff} values and corresponding fatigue crack growth rate response following single overloads at various conditions. Growth rates are normalized by the average steady state rate immediately preceding the overload, while ΔK_{eff} values are normalized by the ΔK values of postoverload cycling--typically 6-8 MPa$\sqrt{m}$. The values of ΔK_{eff} were obtained from measured P_{op}/P_{max} values using Equation 6. As indicated, growth rate measurements made with the SEM at 400X and 1000X were found to be in good agreement with those obtained using the 530X light microscope.

Results in Figure 13 are typical of experiments performed under overload conditions such that $K_{OL}/K_{Ic} < 0.5$ in that no period of accelerated crack growth during, or immediately following, the overload was observed. On the other hand, experiments where $K_{OL}/K_{Ic} \sim 1$ resulted in a pronounced acceleration period, as shown in Figures 14 and 15. In fact, SEM measurements during these tests revealed 30-40 μm of crack extension during the overload cycle itself.

A comparison of results from experiments shown in Figures 14 and 15 is interesting. The main feature which differs between these experiments is that the latter contained an underload to near-zero load immediately following the overload; this half-cycle significantly decreased the transient fatigue crack growth rate response and measured ΔK_{eff} values. Correspondingly, N_D is also decreased from 16 kc to 4.5 kc. In the experiment without the underload, no crack growth was observed over a period of about 500 cycles after the crack had extended about 0.1 mm beyond the crack length at the overload; it is estimated that the crack growth rate was less than 2×10^{-9} m/cycle during this period or about 1000X slower than the steady state rate observed before the overload, Figure 14. By contrast, the growth rates following the overload/underload experiment were reduced by not more than about 3X, Figure 15.

Certain aspects of the change in ΔK_{eff} following the overload are as one might expect. Immediately after the overload, ΔK_{eff} increased due to the extensive blunting of the overload cycle, recall Figure 10(b).

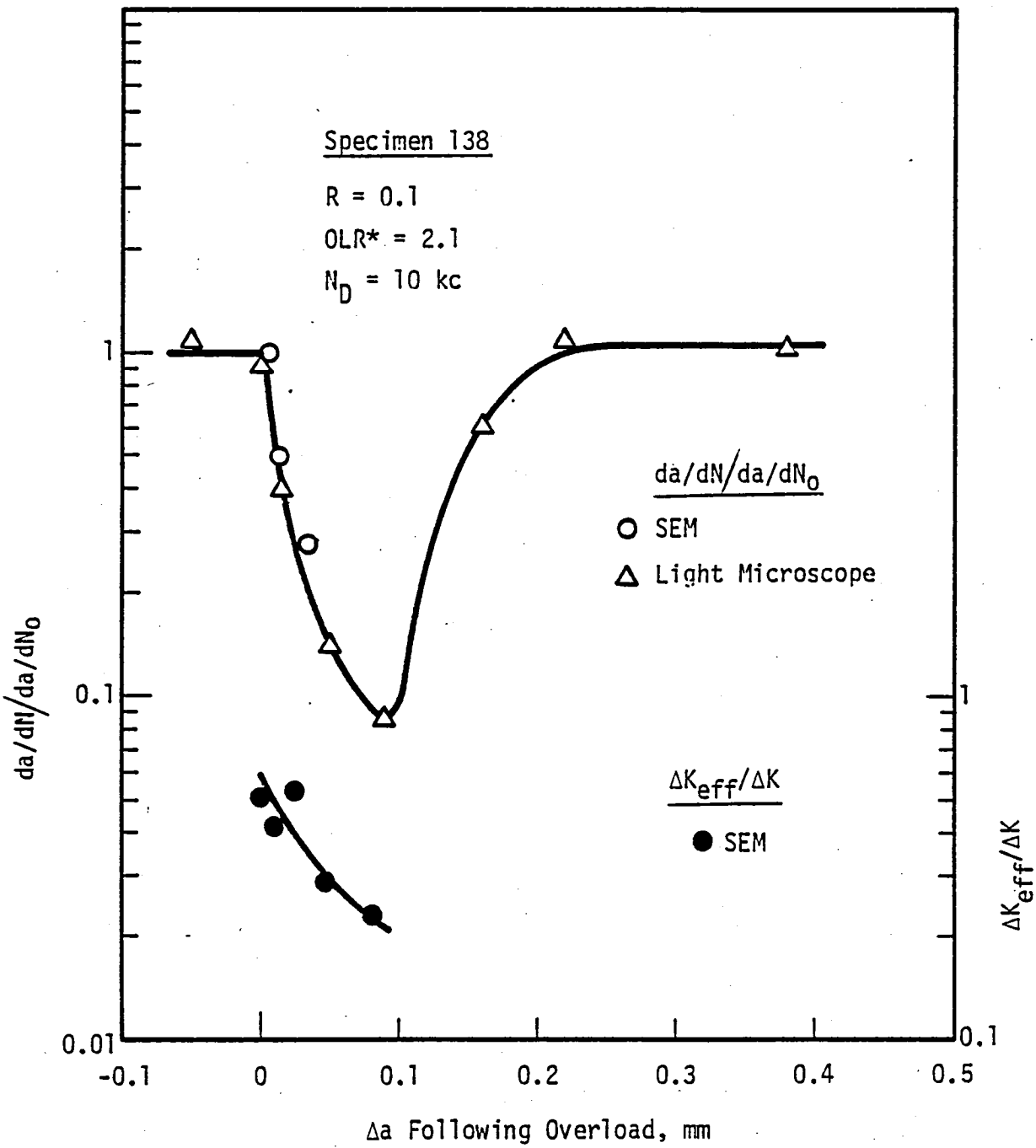

FIGURE 13. MEASURED CRACK GROWTH RATE RESPONSE AND ΔK_{eff} FOLLOWING A SINGLE OVERLOAD AT R = 0.1, OLR* = 2.1

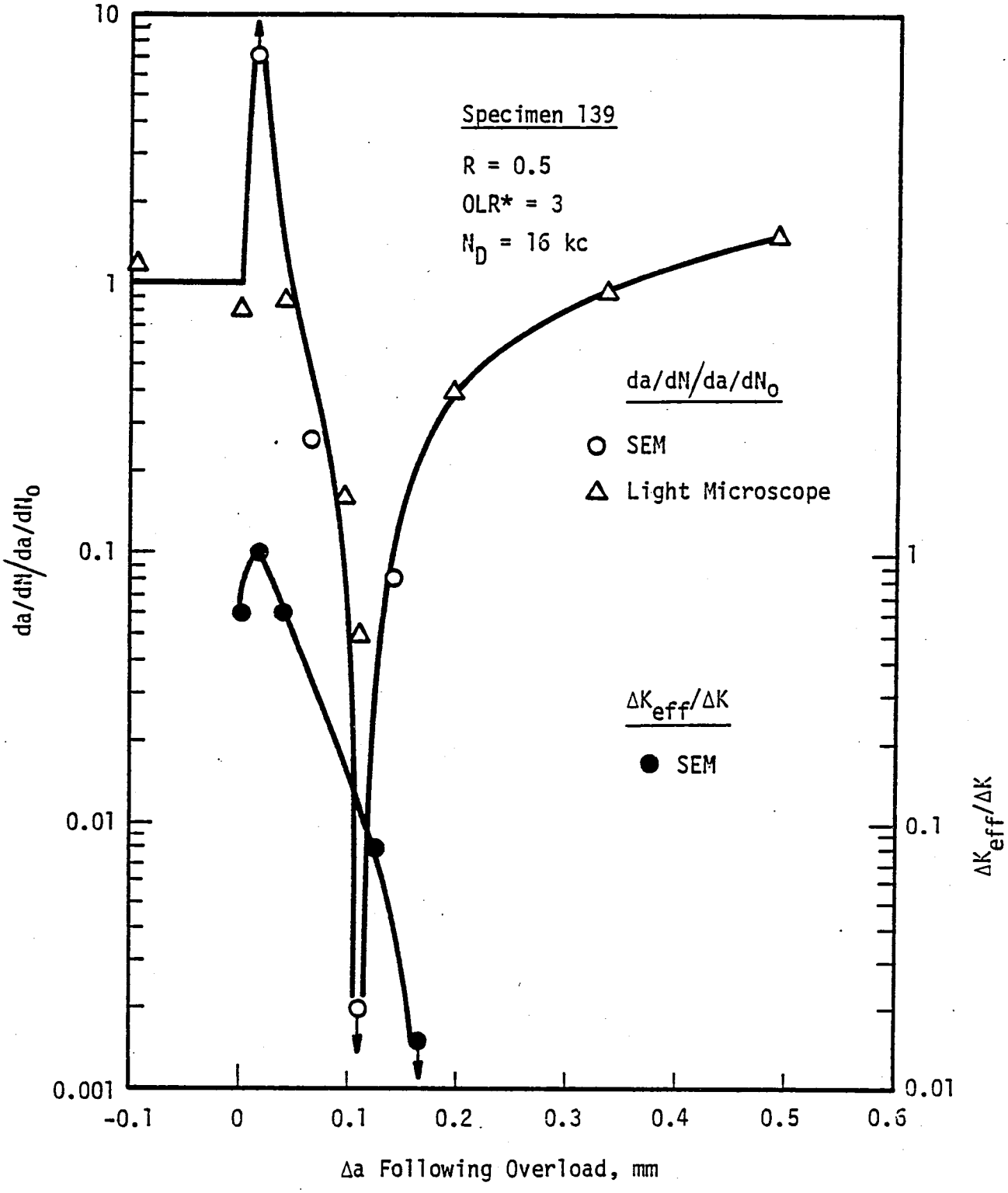

FIGURE 14. MEASURED CRACK GROWTH RATE RESPONSE AND ΔK_{eff} FOLLOWING A SINGLE OVERLOAD AT R = 0.5, OLR* = 3

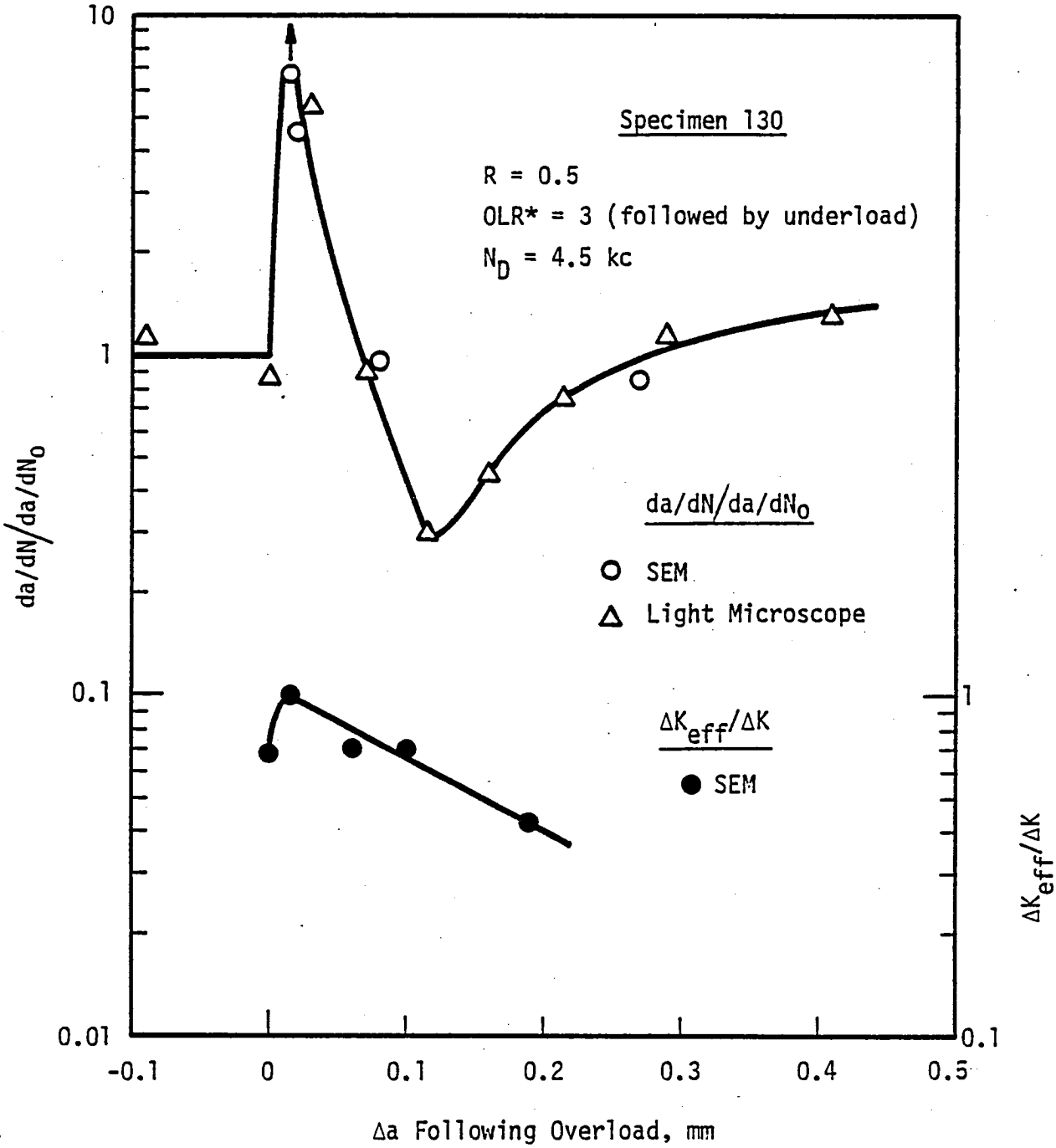

FIGURE 15. MEASURED CRACK GROWTH RATE RESPONSE AND ΔK_{eff} FOR A SINGLE OVERLOAD FOLLOWED BY AN UNDERLOAD TO NEAR ZERO (R = 0.5, OLR* = 3)

This sudden increase is followed by a steady decrease in ΔK_{eff} as the crack grows ever slower into the overload plastic zone. In certain experiments, $P_{op} \sim P_{max}$; thus, no ΔK_{eff} could be measured, Figure 14. Although ΔK_{eff} eventually recovered to its preoverload value, these measurements were ordinarily not obtained.

Although the above response in ΔK_{eff} following the overload is generally consistent with the crack growth rate response, certain behavior is inconsistent. Specifically, the minimum ΔK_{eff} did not occur at precisely the same crack length as did the minimum da/dN value, particularly at high R and OLR* values. Consequently, there exist regimes where da/dN is increasing while ΔK_{eff} is still decreasing; for example, see Figures 14 and 15. A similar trend has been reported by Brown and Weertman [25] in 7050-T76 aluminum. This trend is believed to be associated with the three-dimensional nature of the crack growth retardation problem. Specifically, these results suggest that the transient growth rates following overloads are controlled by the through-thickness average value of the crack-opening load rather than by the surface crack-opening load. Unfortunately, the former cannot be reliably determined.

5.0 ANALYTICAL RESULTS AND DISCUSSION

Two analytical models for crack closure were considered. Both models utilize the Dugdale strip yield formulation [52] and assume rigid-perfectly plastic material behavior. The first model is based solely on crack-tip residual stress and was developed in the current study. The second model is based on plastic deformation in the wake of the advancing crack and was developed by Newman [50, 51].

5.1 Residual Stress Model

The residual stress model for crack closure is based on Rice's [60] original concept of reversed yielding at the crack tip during fatigue crack growth. A detailed derivation of this model is provided in the Appendix. For constant amplitude loading, the normalized effective ΔK is simply given by

$$(\Delta K_{eff}/\Delta K)_{C.A.} = 1 - 4\sqrt{2\alpha'/\pi} \qquad (7)$$

where α' is a measurable, dimensionless constant given by $\alpha' = \omega/(\Delta K/\sigma_{ys})^2$ and ω is the cyclic plastic zone size. Interestingly, Equation 7 predicts that $\Delta K_{eff}/\Delta K$ is a constant value, independent of load ratio. Measurement of α' for a 6061-T6 aluminum alloy using selected area electron channeling gives a value of 0.016 [29, 61]. Using $\alpha' = 0.016$ in Equation 7 gives

$$(\Delta K_{eff}/\Delta K)_{C.A.} = 0.61 \qquad (8)$$

This value is plotted in Figure 7 along with the measured values of $\Delta K_{eff}/\Delta K$. As indicated, the predicted value is in reasonable agreement with measurements at R = 0.33 and 0.5, but overestimates ΔK_{eff} at lower R values.

It is instructive to compare the measured value of α' with analytical estimates of this constant. First, however, it should be recognized that crack closure undoubtedly occurred in the experiments used to measure α', but was not accounted for in analytical estimates of this constant [60]. Since measurements were performed at low R, $\Delta K_{eff}/\Delta K$ for these experiments should be about 0.45, based on results in Figure 7, thereby giving

$$\alpha'' = \alpha' \left(\frac{\Delta K}{\Delta K_{eff}} \right)^2 = 0.079$$

where $\alpha'' = \omega/(\Delta K_{eff}/\sigma_{ys})^2$. This value of α'' is in good agreement with Rice's analytical estimate for plane stress (0.080), but nearly three times larger than that for plane strain (0.027).

The value of ΔK_{eff} associated with an overload can be derived in analogous fashion to the above constant amplitude case and is given in the Appendix. However, in this case, ΔK_{eff} will depend on the magnitude of the overload, OLR*, as follows:

$$(\Delta K_{eff}/\Delta K)_{OL} = 1 - 4\ OLR^* \sqrt{2\alpha'/\pi} \qquad (9)$$

where $OLR^* = \Delta K_{OL}/\Delta K$, as previously defined. For OLR* = 2.1 and $\alpha' = 0.016$, Equation 9 predicts $(\Delta K_{eff}/\Delta K)_{OL} = 0.15$. This value represents a reasonable lower bound on the measured $\Delta K_{th}/\Delta K$ values following an overload at OLR* = 2.1, Figure 13. It is reasonable that Equation 9 should give a minimum value for $\Delta K_{th}/\Delta K$ since perfectly plastic material behavior is assumed in this simple model. The measured gradient in $\Delta K/\Delta K_{th}$ as the crack grows into the overload plastic zone is likely due to strain hardening in the actual test material.

Equation 9 can be used to predict the value of OLR* corresponding to crack arrest following an overload by setting $\Delta K_{th}/\Delta K = 0$ and solving to give

$$(OLR^*)_{arrest} = \frac{1}{4\sqrt{2\alpha'/\pi}} \qquad . \qquad (10)$$

Again, using $\alpha' = 0.016$ gives $(OLR^*)_{arrest} = 2.5$. This prediction seems appropriate for many I/M aluminum alloys [9, 16, 26], but not for X7091-T7E69 tested in the current program where arrest was not observed for OLR* values up to 3.25. This apparent discrepancy may be due to the fact that α' for X7091-T7E69 is less than 0.016, the value for 6061-T3 which was used in the above calculations.

5.2 Plastic Wake Model

The plastic wake model for crack closure examined herein was that developed by Newman [50, 51]. Similar models have been formulated by Fuhring and Seeger [45-47] and others [44, 48]. In all cases, residual plastic deformation along the crack flanks, as well as deformation within the plastic zone, are represented by a series of one-dimensional material elements. The deformation state of these elements is monitored cycle-by-cycle and compared with the elastic displacements of the crack flanks. Contact (or closure) stresses arise when the size of the deformed elements is greater than the computed elastic displacements. The crack opening stress (or load) is given by the point where the crack surfaces become fully opened and the contact stress becomes zero. Newman's model also considers the effect of stress state on the deformation of uncracked elements (within the crack-tip plastic zone) through the use of a constraint factor, α, which can vary from one (plane stress) to three (plane strain). This factor elevates the materials' flow stress for crack-tip elements, thereby simulating the effect of three-dimensional constraint exerted by elastic material surrounding the crack tip. Although crack-tip residual stresses arising from crack-tip plastic strains are computed, they are assumed to have no effect on the crack opening load. Herein lies the difference between the plastic wake model and the residual stress model.

Computations using the above model were conducted using the FAST-2 (Fatigue-Crack Growth Analysis of Structures - A Closure Model) computer program made available to SwRI by Dr. J. C. Newman of NASA-Langley. This program was installed on a DEC PDP 11/70 digital computer.

The model was initially executed to predict the steady state crack opening stress, and thereby ΔK_{eff}, for constant amplitude fatigue crack growth at a variety of R values. Input to this analysis included specimen and crack geometry, material strength properties, constraint factor, and loading conditions. The latter conditions were selected to produce equivalent ΔK values in the center cracked geometry used in the model and the single-edge-notched geometry used in the experiments. Thus, it is implicitly assumed that the analytical predictions are insensitive to specimen geometry. Predictions of normalized crack opening loads and ΔK_{eff} using the model are given in Figures 6 and 7, respectively. As indicated, predictions were in best agreement with measurements when plane stress ($\alpha = 1$) conditions were assumed.

A critical test for the utility of the model for variable amplitude loading is to compare the predicted and measured response in crack growth rate and ΔK_{eff} values following single overloads, particularly for varying R values (as in Figures 13-15). In order for the analytical model to predict this response, additional information is required; namely, a criterion for crack advance and a kinetic equation which relates da/dN to the mechanical driving force--taken here to be ΔK_{eff}. The crack advance criterion in the FAST-2 model is simply formulated in terms of the maximum plastic zone size as follows:

$$\Delta c^* = 0.05\,(1-R)^2\,\rho_{max} \qquad (11)$$

where $(1-R)^2\,\rho_{max}$ is proportional to the cyclic plastic zone size†, Δc^* is the crack growth increment, and 0.05 is a somewhat arbitrary constant selected to be large enough to give reasonable computation times but small enough to provide results which were not markedly sensitive to Δc^*.

The equation relating da/dN to ΔK_{eff} in FAST-2 was developed to describe the complete range of crack growth rates from the threshold

---

† This crack growth criterion is a recent alteration of the FAST-2 model and thereby differs from that based on the monotonic plastic zone size used in Reference 50.

stress intensity factor range, ΔK_{th}, to final instability and is given by the following asymptotic relation:

$$\frac{dc}{dN} = C_1 \Delta K_{eff}^{C_2} \frac{1 - \left(\frac{\Delta K_o}{\Delta K_{eff}}\right)^2}{1 - \left(\frac{K_{max}}{C_5}\right)^2} \tag{12}$$

where

$$\Delta K_o = C_3\left[1 - C_4\left(\frac{S_o}{S_{max}}\right)\right]$$

$$K_{max} = S_{max}\sqrt{\pi c}\ F$$

$$\Delta K_{eff} = (S_{max} - S_o)\sqrt{\pi c}\ F$$

and

C_1 = Crack-growth coefficient (= 1.5×10^{-9})
C_2 = Crack-growth power (= 3.65)
C_3 = Threshold constant (= 1 MPa$\sqrt{m}$)
C_4 = Threshold constant (= 0)
C_5 = Cyclic fracture toughness (= 34 MPa$\sqrt{m}$)
S_{max} = Maximum applied stress (= 57.3 MPa)
S_o = Crack-opening stress (computed)
c = Current crack length (computed)
F = Boundary-correction factor (computed)
K_{max} = Maximum stress intensity factor (computed).

The specific values given above in parentheses were obtained from the constant amplitude fatigue crack growth rate data on X7091-T7E69 shown in Figure 4.

Difficulties were encountered upon implementing the FAST-2 program for the overload sequences. Predicted values of opening stress were unstable--that is, they oscillated wildly--and crack arrest occurred unexpectedly under certain conditions. It was concluded that incompatibilities existed between the FAST-2 program and the PDP 11/70 computer. Resolution of this problem was beyond the scope of the current program; thus, computation of crack opening stress, ΔK_{eff}, and da/dN were pursued no further at this time.

6.0 GENERAL DISCUSSION

Although the emphasis of this study was on variable amplitude crack growth, examination of the simpler case of constant amplitude crack growth is extremely useful since an understanding of this problem is a prerequisite to understanding the more complex case of variable amplitude crack growth. Consider the comparison between measured and predicted values of ΔK_{eff} as a function of R, for constant amplitude crack growth at ΔK = 6-8 Mpa$\sqrt{m}$, as shown in Figure 7. Reasonably good agreement was observed between analytical predictions from the plastic wake model and ΔK_{eff} measurements at R = 0.1, 0.33, and 0.5. Interestingly, however, predictions from the residual stress model were also in reasonable agreement with measurements at R values of 0.33 and 0.5, while they overestimate ΔK_{eff} at R = 0.1. Furthermore, the residual stress model predicts that, very local to the crack tip, crack closure may occur even at high R values. Based on these results, it is hypothesized that the plastic wake effects control crack closure at low R values, but that crack-tip residual stresses become increasingly important as R values increase above R = 0.5. Thus, the obvious critical experiments are to extend results of the current study to higher R values--for example, $R \geq 0.7$.

The above hypothesis is also consistent with the data obtained on the delay characteristics of X7091-T7E69 as a function of overload magnitude (OLR*) and R. As shown in Figure 9, results at R = 0.33 and 0.5 are not measurably different, while those at R = 0.1 give delay periods which are about a factor of two greater than those at higher R values. These results are consistent with the increasing importance of residual stress as R increases. Under single overloads, the residual stress model predicts that ΔK_{eff} is dependent only on the magnitude of the overload (OLR*) and independent of R. On the other hand, the plastic wake model would predict a systematic increase in delay cycles as R is increased.

We fully recognize the controversy surrounding the concept of compressive residual stresses, ahead of the crack tip, contributing to crack

closure, In fact, certain analyses indicate the opposite--that is, that compressive stresses within the cyclic plastic zone tend to open rather than close the crack tip [60]. However, these results may reflect the inadequacy of current analytical techniques to treat the complexities of a growing fatigue crack, rather than negate the concept of residual stresses contributing to crack closure. Observation made in the SEM of surface fatigue cracks growing through residual stress fields supports the concept that compressive residual stresses can contribute to crack closure [63]. As previously mentioned, measurements of ΔK_{eff} at high R-values will help to resolve this problem.

It is instructive to compare the SEM measurements of ΔK_{eff} with measurements from other studies. The measured ΔK_{eff} values at low R in Figure 7 are about one-half those reported by McEvily in P/M alloys X7071-T7E69 and X7090-T6 for ΔK = 6-8 MPa$\sqrt{m}$ [64]. McEvily's measurements were obtained using elastic compliance measured remote from the crack tip. This difference in results between the two studies is at least partially due to the fact that SEM measurements are sensitive to processes in the near-crack-tip region, while remote techniques which measure the global specimen response cannot detect processes local to the crack tip. In addition, the latter provides a measure of average through-thickness specimen response, while the SEM measurements may only be measuring the response dominated by the plane stress region at the specimen surface. (This view is supported by agreement between measured and predicted ΔK_{eff} values only when plane stress conditions are assumed, as well as by the agreement between measured and predicted cyclic plastic zone size, provided crack closure is taken into account.) Crack closure and crack growth retardation are known to be dominated by the plane stress surface response as indicated indirectly by increasing delay periods with decreasing specimen thickness [9, 14, 15, 19-23], as well as directly by significant reductions in crack closure when plane stress surface regions are removed by machining subsequent to fatigue crack extension [65]. Using both remote (average) and local (surface) crack closure measurements in complementary fashion would seem to be useful in quantifying these three-dimensional, stress state effects.

The current study has also demonstrated that the period of eventual crack growth deceleration corresponds to a marked decrease in ΔK_{eff}. However, the minimum crack growth rate during this period occurs before the minimum ΔK_{eff} is achieved, for example see Figures 14 and 15. This apparent "phase shift" is also believed to be a manifestation of the three-dimensional nature of the problem. Specifically, the surface measurements reflect primarily the plane stress crack opening response; however, the growth rate responds to the average through-thickness "driving force." Here again a comparison of remote (average) and local (surface) crack closure measurements would help to resolve this apparent dichotomy. A fractographic study of possible through-thickness variations in the size of the stretch zone formed during the overload cycle should also contribute to an improved understanding of this issue.

7.0 SUMMARY AND CONCLUSIONS

The following conclusions are drawn based on the experimental work on X7091-T7E69 aluminum and compansion analytical modeling:*

1. Microscopic measurements, obtained with a SEM using stereoimaging, show that constant amplitude fatigue crack growth (at ΔK = 6-8 MPa$\sqrt{m}$) produces crack-tip opening loads (P_{op}) which are 1.4 to 6 times greater than the minimum applied load in the cycle (P_{min}), increasing as the load ratio (R) decreases from 0.5 to 0.1. Correspondingly, $\Delta K_{eff}/\Delta K$ values decrease from 0.64 to 0.45 as R is decreased from 0.5 to 0.1.

2. For constant amplitude crack growth, the agreement between observed P_{op} and ΔK_{eff} values and those predicted from a plane stress crack closure model, as well as agreement between reported values of the cyclic plastic zone size and plane stress analytical estimates, suggest that SEM measurements made at the specimen surface are associated with a state of plane stress.

3. Microscopic measurements of ΔK_{eff} (at ΔK = 6-8 MPa$\sqrt{m}$) using the SEM are observed to be about one-half of the values reported using global techniques such as elastic compliance or electrical potential. This difference is partially caused by the fact that SEM measurements are

---

* Caveat: Subsequent to the preparation of this report, it came to our attention that the split-pin, wedge-loading technique, periodically used to maintain a mean load on the specimen, may have allowed partial unloading near the crack tip. This periodic unloading has the potential to reduce the measured delay cycles at high-R and correspondingly alter the crack growth transients and associated ΔK_{eff} measurements. A combined analytical and experimental effort is planned to examine the consequencies of this effect on the results and conclusions of the current study.

sensitive to processes in the near crack-tip region, while global techniques cannot detect these local processes. In addition, the latter provide a measure of average through-thickness behavior, while the SEM measurements are at the specimen surface--a region of lesser constraint than the mid-thickness of the specimen. Nevertheless, since three-dimensional considerations are an important aspect of crack closure and crack growth retardation, the two types of measurements are complementary.

4. Crack-tip measurements of P_{op} and ΔK_{eff} as a function of R for constant amplitude crack growth are in reasonable agreement with plane stress predictions based on classical plastic wake concepts of crack closure. However, observations of growing cracks in the SEM, as well as results from a residual stress model suggest that crack-tip residual stresses within the cyclic plastic zone also contribute to crack closure, becoming increasingly important as R increases. This suggests that very near the crack tip, closure may occur even at high R values even though the crack flanks are not in contact. This hypothesis needs to be confirmed by critical measurements of P_{op} and ΔK_{eff} at $R > 0.7$.

5. Single overloads initially produce crack-tip blunting which temporarily eliminates crack closure and is accommodated by the emergence of intense shear bands from the deformed crack tip. This process can result in crack growth acceleration (provided K_{OL} is a significant fraction of K_{IC}) which corresponds to crack extension along the predominant shear band. This process occurs in both P/M and I/M alloys, thus it appears to be a general feature of crack growth following overloads in

aluminum alloys. At high R values this process occurs over a significant portion of the overload-affected zone, especially when the magnitude of the overload (OLR*) is relatively small.

6. The period of eventual crack growth deceleration following an overload corresponds to a decrease in ΔK_{eff}. However, the minimum growth rate during this period is achieved before the minimum ΔK_{eff} occurs. This apparent phase shift has also been observed using global measurements. This apparent difference is likely to be due to the fact that the driving force for crack growth is the average through-thickness ΔK_{eff} value, whereas the SEM measurements reflect lower ΔK_{eff} values associated with the plane stress surface region.

7. At a given value of OLR*, the number of delay cycles, N_D, tends to decrease with increasing R. In X7091-T7E69, increasing R from 0.1 to 0.33 decreases N_D by about a factor of two, however no measurable change in N_D occurs between R of 0.33 and 0.5, thereby suggesting saturation. These results appear to be inconsistent with the classical plastic wake mechanism of crack closure and reflect the increased significance of crack-tip residual stress at high R values (see Conclusions 4 and 9).

8. At R = 0.1, P/M aluminum alloy X7091-T7E69 exhibited less delay than a variety of I/M aluminum alloys. At this low R value, this behavior may be related to the occurrence of less crack closure in the P/M alloy due to its smooth fracture surface morphology and thus low asperity contact. These results are in contrast to reports of superior performance of the P/M alloys under certain specific spectra, and attest to the need for additional fundamental work on the influence of material/ microstructural variables on variable amplitude crack growth.

9. It is recommended that this study be followed up by predictions based on the plastic wake model of crack closure (FAST-2). Comparisons of measured and predicted values of N_D, da/dN-transients, and ΔK_{eff} following overload will provide critical tests for the model, as well as strengthen or negate certain of the above conclusions.

8.0 REFERENCES

1. J. Schijve, "Fatigue Crack Propagation in Light Alloy Sheet Material and Structures," Rept. MP 195, National Luchtvaartlaboratorium, Amsterdam, The Netherlands, August, 1960.

2. C. M. Hudson and H. F. Hardrath, "Effects of Changing Stress Amplitude on the Rate of Fatigue Crack Propagation of Two Aluminum Alloys," NASA Technical Note D-960, National Aeronautics and Space Administration, 1961.

3. C. M. Hudson and H. F. Hardrath, "Investigation of Variable Loadings of Fatigue Crack Propagation Patterns," NASA Technical Note D-1803, National Aeronautics and Space Administration, 1963.

4. R. H. Christensen, Proceedings - Crack Propagation Symposium, Cranfield, College of Aeronautics, 1962.

5. O. Jonas and R. P. Wei, An Exploratory Study of Delay in Fatigue Crack Growth, Int. J. Fract., p. 116, 1971.

6. J. Schijve and D. Broek, "The Results of a Test Programme Based on A Gust Spectrum with Variable Amplitude Loading," Aircraft Engineering, Vol. 34, p. 1962.

7. W. Elber, "The Significance of Fatigue Crack Closure," in Damage Tolerance in Aircraft Structures, ASTM STP 486, p. 230, 1971.

8. W. T. Matthews, F. I. Baratta and G. W. Driscoll, Intl. J. Fracture Mechanics, Vol. 7, p. 224, 1971.

9. E. F. J. von Euw, R. W. Hertzberg and R. Roberts, "Stress Analysis and Growth of Cracks, ASTM STP 513, p. 230, 1972.

10. C. M. Hudson and K. N. Raju, "Investigation of Fatigue Crack Growth Under Simple Variable Amplitude Loading," NASA Technical Note D-5702, National Aeronautics and Space Administration, 1970.

11. V. W. Trebules, Jr., R. Roberts and R. W. Hertzberg, "Effect of Multiple Overloads on Fatigue Crack Propagation in 2024-T3 Aluminum Alloy," in Progress in Flaw Growth and Fracture Toughness Testing, ASTM STP 536, p. 115, 1973.

12. D. M. Corbly and P. F. Packman, "On the Influence of Single and Multiple Peak Overloads and Fatigue Crack Propagation in 7075-T6511 Aluminum," Engineering Fracture Mechanics, Vol. 5, p. 497, 1973.

13. R. P. Wei, T. T. Shih and J. H. Fitzgerald, "Load Interaction Effects on Fatigue Crack Growth in Ti-6Al-4V Alloy," NASA CR-2239, April 1973.

14. R. P. Wei and T. T. Shih, "Delay in Fatigue Crack Growth," Int. J. Fract., 10(1), pp. 77-85, 1974.

15. T. T. Shih and R. P. Wei, "A Study of Crack Closure in Fatigue," Engng. Fract. Mech., 6, pp. 19-32, 1974.

16. G. R. Chanani, "Fundamental Investigation of Fatigue Crack Growth Retardation in Aluminum Alloys," Technical Report AFML-TR-76-156, Air Force Materials Laboratory, Wright-Patterson Air Force Base, OH, September 1976.

17. C. Bathias and M. Vancon, "Mechanism of Overload Effect on Fatigue Crack Propagation in Aluminum Alloys," Engr. Fracture Mechanics, Vol. 10, p. 409, 1978.

18. E. P. Probst and B. M. Hillberry, "Fatigue Crack Delay and Arrest Due to Single Peak Tensile Overloads," AIAA Journal, Vol. 12, No. 3, p. 330, March 1974.

19. T. T. Shih and R. P. Wei, "Effect of Specimen Thickness on Delay in Fatigue Crack Growth," J. Testing and Evaluation, ASTM, Vol. 3, p. 46, 1975.

20. W. J. Mills and R. W. Hertzberg, "The Effect of Sheet Thickness on Fatigue Crack Retardation in 2024-T3 Aluminum Alloy," Engr. Fracture Mechanics, Vol. 17, p. 705, 1975.

21. T. T. Shih and R. P. Wei, ASTM STP 595, p. 113, 1976.

22. G. R. Chanani, "Effect of Thickness on Retardation Behavior of 7075 and 2024 Aluminum Alloys," in Flaw Growth and Fracture, ASTM STP 631, p. 365, 1977.

23. S. Matsuoka and K. Tanaka, "The Influence of Sheet Thickness on Delayed Retardation Phenomena in Fatigue Crack Growth in HT80 Steel and A5083 Aluminum Alloy," Engr. Fracture Mechanics, Vol. 13, p. 293, 1980.

24. R. P. Wei, N. E. Fenelli, K. D. Unangst, and T. T. Shih, "Fatigue Crack Growth Response Following a High-Load Excursion in 2219-T851 Aluminum Alloy," J. Eng. Mat. Tech., Trans. ASME, 102, p. 280, 1980.

25. R. D. Brown and J. Weertman, "Effects of Tensile Overloads on Crack Closure and Crack Propagation Rates in 7050 Aluminum," Engr. Fracture Mechanics, Vol. 10, p. 867, 1978.

26. M. K. Himmelein and B. M. Hillberry, "The Effect of Stress Ratio and Overload Ratio on Fatigue Crack Delay and Arrest Behavior Due to Single Peak Overloads," ASTM STP 560, 1976.

27. W. Elber, "The Significance of Fatigue Crack Closure," in Damage Tolerance of Aircraft Structures, ASTM STP 486, p. 230, 1971.

28. W. Elber, "Fatigue Crack Closure Under Cyclic Tension," Engr. Fract. Mech., 2, p. 37, 1970.

29. J. Lankford and D. L. Davidson, "Fatigue Crack Tip Plasticity Associated with Overloads and Subsequent Cycling," J. Engng. Mat. Tech., Trans. ASME, 98, p. 17, 1976.

30. D. L. Davidson and J. Lankford, "Fatigue Crack Tip Plasticity Resulting from Load Interactions in an Aluminum Alloy," Fat. Engng. Mater. Struct., Vol. 1, p. 439, 1979.

31. J. Lankford and D. L. Davidson, "The Effect of Overloads Upon Fatigue Crack Tip Opening Displacement and Crack Tip Opening/Closing Loads in Aluminum Alloys," in Advances in Fracture Research, D. Francois et al, editors, Vol. 2, Pergamon Press, p. 899, 1981.

32. S. Suresh, "Crack Growth Retardation Due to Micro-Roughness: A Mechanism for Overload Effects in Fatigue," Scripta Met., 16, No. 8, p. 995, 1982.

33. R. E. Jones, "Fatigue Crack Growth Retardation After Single Cycle Peak Overload in Ti-6Al-4V Titanium Alloy," Engr. Fract. Mech., Vol. 5, p. 585, 1973.

34. O. E. Wheeler, "Spectrum Loading and Crack Growth," J. Basic Engng., Trans. ASME, Series D, Vol. 94, p. 181, 1972.

35. J. Willenborg, R. M. Engle and H. A. Wood, "A Crack Growth Retardation Model Using an Effective Stress Intensity Concept," Technical Report AFFDL-TM-71-1-FBR, Air For Flight Dynamics Lab., Wright-Patterson Air Force Base, OH, January 1971.

36. J. P. Gallagher and T. F. Hughes, "Influence of Yield Strength on Overload Affected Fatigue Crack Growth Behavior in 4340 Steel," AFFDL-TR-74-27, Air Force Flight Dynamics Lab., Wright-Patterson Air Force Base, OH, July 1974.

37. J. P. Gallagher and H. D. Stalnaker, "Methods for Analyzing Fatigue Crack Growth Rate Behavior Associated with Flight-by-Flight Loading," J. Aircraft, Vol. 12, p. 699, 1975.

38. W. S. Johnson, "Multi-Parameter Yield Zone Model for Predicting Spectrum Crack Growth," NASA TM 81890, National Aeronautics and Space Administration, September 1980.

39. J. C. Newman, Jr., "Finite-Element Analysis of Fatigue Crack Propagation - Inclusing the Effects of Crack Closure," Ph.D. Thesis, VPI&SU, Blacksburg, VA, May 1974.

40. J. C. Newman, Jr., and Harry Armen, Jr., "Elastic-Plastic Analysis of a Propagating Crack Under Cyclic Loading," AIAA Journal, Vol. 13, No. 8, p. 1017, 1975.

41. K. Obji and Y. Ohkubo, "Cyclic Analysis of a Propagating Crack and Its Correlation with Fatigue Crack Growth," Engineering Fracture Mechanics, Vol. 7, pp. 457-464, 1975.

42. J. C. Newman, Jr., "A Finite-Element Analysis of Fatigue-Crack Closure," Mechanics of Crack Growth, ASTM STP-590, American Society for Testing and Materials, p. 281, 1976.

43. K. Ogura and K. Obji, "FEM Analysis of Crack Closure and Delay Effects in Fatigue Crack Growth Under Variable Amplitude Loading," Engr. Fract. Mech., Vol. 9, p. 471, 1977.

44. B. Budiansky and J. W. Hutchinson, "Analysis of Closure in Fatigue Crack Growth," J. Appl. Mech., Vol. 45, p. 267, 1978.

45. H. Fuhring and T. Seeger, "Acceleration and Retardation Effects with Fatigue Crack Growth and Their Calculation Based on Fatigue Fracture Mechanics," in Proc. 2nd Int. Conf. on Mechanical Beh. of Mat., p. 721, 1976.

46. H. Fuhring and T. Seeger, "Dugdale Crack Closure Analysis of Fatigue Cracks Under Constant Amplitude Loading," Engineering Fracture Mechanics, Vol. 11, p. 99, 1979.

47. H. Fuhring and T. Seeger, "Structural Memory of Cracked Components Under Irregular Loading," Fracture Mechanics, ASTM STP-677, p. 144, 1979.

48. H. D. Dill and C. R. Saff, "Spectrum Crack Growth Prediction Method Based on Crack Surface Displacement and Contact Analyses," Fatigue Crack Growth Under Spectrum Loads, ASTM STP-595, p. 306, 1976.

49. H. F. Hardrath, J. C. Newman, Jr., W. Elber, and C. C. Poe, Jr., "Recent Developments in Analysis of Crack Propagation and Fracture of Practical Materials," Fracture Mechanics, edited by N. Perrone, University Press of Virginia, 1978.

50. J. C. Newman, Jr., "A Crack-Closure Model for Predicting Fatigue Crack Growth Under Aircraft Spectrum Loading," in Methods and Models for Predicting Fatigue Crack Growth Under Random Loading, ASTM STP 748, p. 53, 1981.

51. J. C. Newman, Jr., "Prediction of Fatigue Crack Growth Under Variable-Amplitude and Spectrum Loading Using a Closure Model," in Design of Fatigue and Fracture Resistant Structures, ASTM STP 761, p. 255, 1982.

52. D. S. Dugdale, "Yielding of Steel Sheets Containing Slits," Journal Mech. Phys. Solids, Vol. 8, 1960.

53. J. P. Lyle, Jr., and W. S. Cebulak, "Powder Metallurgy Approach for Control of Microstructure and Properties in High Strength and Aluminum Alloys," Metallurgical Transactions A, Volume 6A, p. 699, 1975.

54. J. P. Lyle, Jr., and W. S. Cebulak, "Properties of High Strength Aluminum P/M Products," Metals Engineering Quarterly, February 1974.

55. D. J. Brownhill, R. J. Bucci, S. F. Collis, R. E. Davies, J. C. Kuli, R. C. Malcolm, and G. Sowiuski, "Mechanical Property, Corrosion and Exfoilation Data and P/M Alloys 7090-T7E71 and 7091-T7E69 Extrusions," Alcoa Report No. 56-3978, June 21, 1983.

56. W. F. Brown, Jr. and J. E. Srawley, "Plane Strain Crack Toughness Testing of High-Strength Metallic Materials," ASTM STP 410, American Society for Testing and Materials, 1966.

57. D. L. Davidson and A. Nagy, "A Low Frequency Cyclic Loading Stage for the SEM," J. of Physics, Vol. E11, p. 207, 1978.

58. D. R. Williams, D. L. Davidson and J. Lankford, "Fatigue Crack Tip Plastic Strains by the Stereoimaging Technique," Eng. Mech., Vol. 20, p. 134, 1980.

59. D. L. Davidson, D. R. Williams, J. E. Buckingham, "Crack Tip Stresses as Computed from Strains Determined by Stereoimaging," Exp. Mech., p. 242, June 1983.

60. J. R. Rice, "Mechanics by Crack Tip Deformation and Extension by Fatigue," ASTM STP 415, p. 247, 1967.

61. J. Lankford, D. L. Davidson and T. S. Cook, "Fatigue Crack Tip Plasticity," ASTM STP 637, p. 36, 1977.

62. H. Tada, P. C. Paris and G. R. Irwin, "The Stress Analysis of Cracks Handbook," Del Research Corporation, Hellertown, PA, 1973.

63. J. E. Hack and G. R. Leverant, "Influence of Compressive Residual Stress on the Crack-Opening Behavior of Part-Through Fatigue Cracks," ASTM STP 776, p. 204, 1982.

64. A. J. McEvily, "The Fatigue of Powder Metallurgy Alloys," Annual Report, USAF Grant AFOSR81-0046, University of Connecticut, Storrs, Connecticut, January 1983.

65. G. Marci and P. F. Packman, "The Effects of Plastic Wake Zone on the Conditions for Fatigue Crack Propagation," Int. J. Fract., Vol. 16, 1980.

APPENDIX

A CRACK CLOSURE MODEL BASED ON CRACK TIP RESIDUAL STRESS

A CRACK CLOSURE MODEL BASED ON CRACK-TIP RESIDUAL STRESS

A simple model is developed herein for crack closure based on Rice's [60] concept of crack-tip residual stress developed within the cyclic plastic zone. For simplicity, elastic-perfectly plastic material behavior is assumed. The model contains only one parameter, $\alpha' = \omega/(\Delta K/\sigma_{ys})^2$, where ω is the cyclic plastic zone size. The value of α' can be measured using a variety of experimental techniques [61]. Effective stress intensity factor values are derived for both constant amplitude loading and for single overloads.

A. Constant Amplitude Loading

The crack-tip stress-strain behavior of a growing fatigue crack has been analyzed by Rice [60]. Schematically, Rice's analysis indicates that a monotonic and a cyclic or reverse plastic zone are formed at the tip of the growing crack [see Figure A-1(a) and (b)]. The condition for the onset of reverse plastic flow is illustrated in Figure A-1(b) and it occurs when the stress at the crack-tip is reduced to $-2\ \sigma_{ys}$. Plastic superposition of the stress-strain conditions depicted in Figure A-1(a) and (b) would result in the crack-tip behavior shown in Figure A-1(c).

A different approach is taken in the residual stress model. The cyclic plastic zone and the local stress condition in Figure A-1(b) are approximated by extending the crack by an increment equal to the size of the cyclic plastic zone, ω, which is acted upon by a compressive stress of magnitude equal to $2\ \sigma_{ys}$ (see Figure A-2). The residual stress intensity associated with the partially-loaded crack shown in Figure A-2 can be obtained by using the stress intensity solution reported by Tada et al [62], which is given by the following equation:

$$K_R = -4\sqrt{\frac{2}{\pi}}\ \sigma_{ys}\sqrt{\omega} \quad . \tag{A1}$$

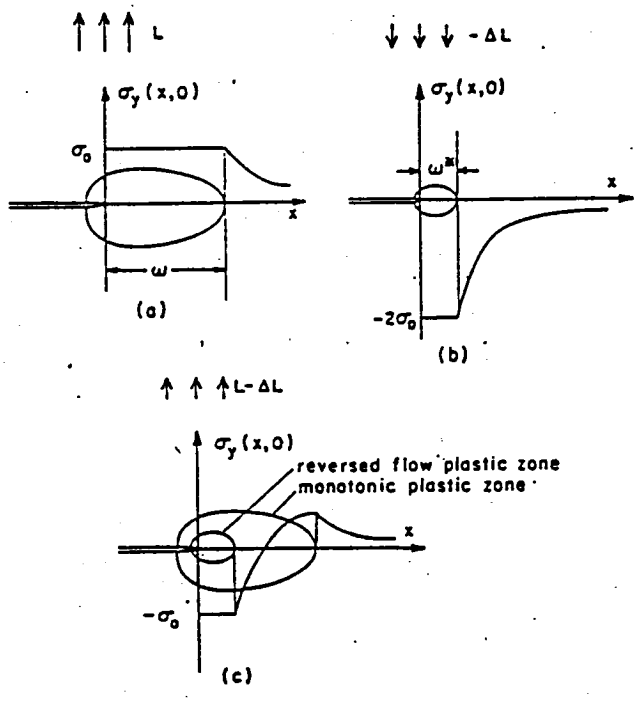

FIGURE A-1. PLASTIC SUPERPOSITION FOR UNLOADING. Adding (b) for load - ΔL with a doubled yield stress to (a) gives the solution (c) resulting after unloading from L to L - ΔL. Reloading, L - ΔL to L, restores (a), taken from [60].

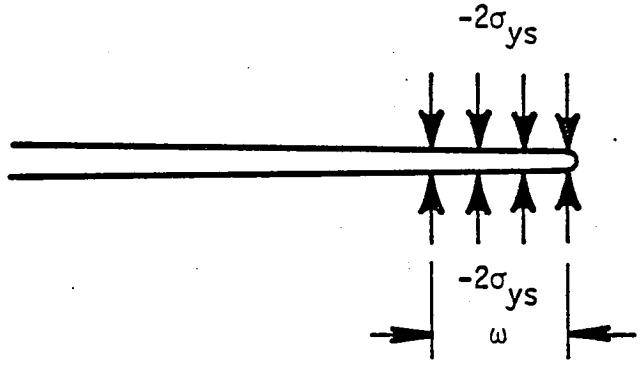

FIGURE A-2. THE RESIDUAL STRESS MODEL

The size of the cyclic plastic zone can be obtained as follows:*

$$\omega = \alpha' \left(\frac{\Delta K}{\sigma_{ys}} \right)^2 \quad . \tag{A2}$$

Substituting Equation A2 into Equation A1, we have

$$K_R = -4 \sqrt{\frac{2\alpha'}{\pi}} \Delta K \quad . \tag{A3}$$

For constant amplitude loading, the driving force for crack growth can be viewed as ΔK, which is reduced by an amount equal to K_R as the result of the presence of residual compressive stresses at the crack tip. Thus, the effective stress intensity range becomes

$$\Delta K_{eff} = \Delta K + K_R$$

$$= \Delta K \left[1 - 4 \sqrt{\frac{2\alpha'}{\pi}} \right] \tag{A4}$$

B. Single Overload

Equation A1 is still applicable after a single overload. The size of the cyclic plastic zone after an overload is, however, increased and is given by

---

* Within the formalism of the residual stress model, σ_{ys} should ideally be the materials' cyclic yield stress, especially for constant amplitude crack growth where material within the cyclic plastic zone is likely to reach steady state cyclic response. The situation is less clear when applying this model to crack growth following an overload where the cyclic zone of interest has only experienced one-half cycle of compressive yielding. Nevertheless, it is more common to find α' values reported in terms of the monotonic yield strength, partly due to lack of data on cyclic yield strengths. Of course, this is not an issue for cyclicly stable materials such as X7091-T7E69.

$$\omega = \alpha' \left(\frac{\Delta K_{OL}}{\sigma_{ys}} \right)^2 \qquad \text{(A5)}$$

where σ_{ys} is the yield strength of the material. Substituting Equation A3 into Equation A1, we have

$$K_{R,OL} = -4\sqrt{\frac{2\alpha'}{\pi}}\, \Delta K_{OL} \quad . \qquad \text{(A6)}$$

Since $\Delta K_{OL} = OLR^* \Delta K$, where OLR* is the overload ratio, Equation A6 becomes

$$K_{R,OL} = -4\sqrt{\frac{2\alpha'}{\pi}}\, \Delta K\, OLR^* \quad . \qquad \text{(A7)}$$

Thus, the effective stress intensity range after a single overload is as follows:

$$\Delta K_{eff,OL} = \Delta K + K_{R,OL}$$

$$= \Delta K \left[1 - 4\ OLR^* \sqrt{\frac{2\alpha'}{\pi}} \right] \quad . \qquad \text{(A8)}$$

1. Report No.	2. Government Accession No.	3. Recipient's Catalog No.
NASA CR-172228		

4. Title and Subtitle	5. Report Date
Measurement and Analysis of Critical Crack Tip Processes Associated with Variable Amplitude Fatigue Crack Growth	September 1983
	6. Performing Organization Code

7. Author(s)	8. Performing Organization Report No.
S. J. Hudak, Jr., D. L. Davidson, and K. S. Chan	SwRI-7042/18
	10. Work Unit No.

9. Performing Organization Name and Address	11. Contract or Grant No.
Southwest Research Institute 6220 Culebra Road P. O. Drawer 28510 San Antonio, Texas 78284	NAS1-16954
	13. Type of Report and Period Covered
12. Sponsoring Agency Name and Address	Contractor Report
National Aeronautics and Space Administration Langley Research Center Hampton, Virginia 23665	14. Sponsoring Agency Code

15. Supplementary Notes

Langley Technical Monitor: Dr. J. C. Newman, Jr.
Final Report

16. Abstract

Crack growth retardation following overloads can result in overly conservative life predictions in structures subjected to variable amplitude fatigue loading when linear damage accumulation procedures are employed. Crack closure is believed to control the crack growth retardation, although the specific closure mechanism has been debatable. The current study provides new information on the relative contributions to crack closure from: 1) plasticity left in the wake of the advancing crack and 2) crack-tip residual stresses. The delay period and corresponding crack growth rate transients following overloads are systematically measured as a function of load ratio (R) and overload magnitude. These responses are correlated in terms of the local "driving force" for crack growth as measured by crack-tip opening loads and ΔK_{eff}. The latter measurements are obtained using a scanning electron microscope equipped with a cyclic loading stage; measurements are quantified using a relatively new stereoimaging technique. Combining experimental results with analytical predictions suggests that both plastic wake and residual stress mechanism are operative, the latter becoming predominate as R increases. Additional critical experiments to further support this hypothesis are recommended.

17. Key Words (Suggested by Author(s))	18. Distribution Statement
Variable amplitude fatigue, Overload effects, Crack closure, Residual stress, Aluminum alloys	Unclassified - Unlimited

19. Security Classif. (of this report)	20. Security Classif. (of this page)	21. No. of Pages	22. Price
Unclassified	Unclassified	70	

For sale by the National Technical Information Service, Springfield, Virginia 22161